

DOCKET NO. 4C 8158

DEPARTMENT OF THE ARMY  
OFFICE OF THE DEPUTY CHIEF OF STAFF FOR LOGISTICS  
WASHINGTON, D.C. 20310

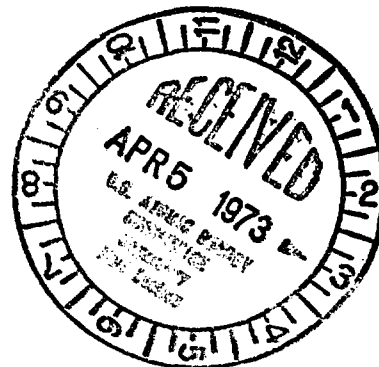
REGULATORY FILE CY



DALO-MAS-I

2 April 1973

U.S. Atomic Energy Commission  
Directorate of Licensing  
Materials Branch  
Washington, D.C. 20545



Gentlemen:

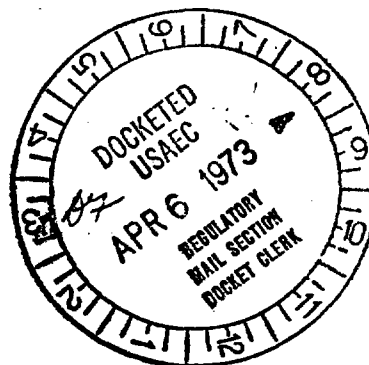
Please refer to USAEC Source Material License No. SUB-1150 issued to the U.S. Army Electronics Command, Fort Monmouth, New Jersey.

Attached is an application to amend this license to add 110 pounds of Thorium 232 contained in sheet metal. Individual pieces of the sheet metal are bonded to the underside of the case of the AN/PDR-56 Radiacmeter to serve as check sources.

Sincerely yours,

*Peter M. Baldino*  
PETER M. BALDINO  
Chief, Support Division

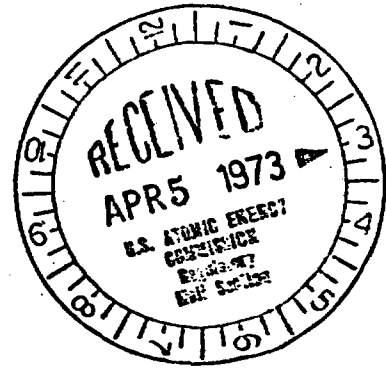
1 Incl  
As stated (4 cys)



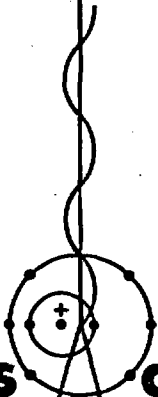
2249  
D/3

LA-4951

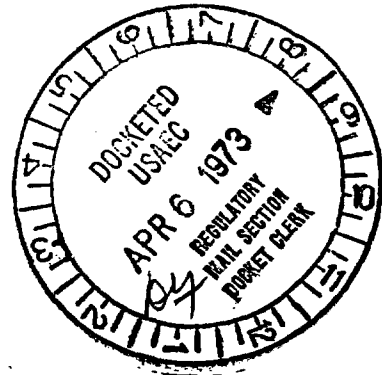
Received W/Ltr. Dated APR 2 1973



Thermal Neutron Irradiation of Sodium-Bonded  
Solid Solution (U,Pu)C Fuel



**Los Alamos**  
**scientific laboratory**  
of the University of California  
LOS ALAMOS, NEW MEXICO 87544



This report was prepared as an account of work sponsored by the United States Government. Neither the United States nor the United States Atomic Energy Commission, nor any of their employees, nor any of their contractors, subcontractors, or their employees, makes any warranty, express or implied, or assumes any legal liability or responsibility for the accuracy, completeness or usefulness of any information, apparatus, product or process disclosed, or represents that its use would not infringe privately owned rights.

Printed in the United States of America. Available from  
National Technical Information Service  
U. S. Department of Commerce  
5285 Port Royal Road  
Springfield, Virginia 22151  
Price: Printed Copy \$3.00; Microfiche \$0.95

LA-4951

UC-79b

ISSUED: February 1973



# Thermal Neutron Irradiation of Sodium-Bonded Solid Solution (U,Pu)C Fuel\*

by

J. C. Clifford\*\*

\*Work supported by the U.S. AEC Division of Reactor Development and Technology.

\*\*Present address: Esso Research, Linden, New Jersey.

# THERMAL NEUTRON IRRADIATION OF SODIUM-BONDED SOLID SOLUTION (U,Pu)C FUEL

by

J. C. Clifford

## ABSTRACT

Small amounts of pelletized, single-phase, uranium-plutonium carbide, sodium-bonded to Type 316 stainless steel cladding, were irradiated in a thermal flux to determine whether fuel, clad, and sodium would remain mutually compatible as burnup progressed. Uranium for the fuel was fully enriched in  $^{235}\text{U}$ , producing a surface-to-centerline fission ratio of  $\sim 12:1$ . During these irradiations, the maximum fuel surface operating temperature was  $730^\circ\text{C}$ , the maximum power density was  $760\text{ W/g}$ , and the maximum burnup attained was  $13\text{ at.}\%$ . These figures are based on fission events only.

The irradiated fuel showed no evidence of attack by sodium and no other surface changes, although extensive cracking, sodium logging, and a noble fission-product-containing phase were observed in various samples. The cladding on inside surfaces showed evidence of light, intermittent carburization at all operating temperatures ( $600$  to  $720^\circ\text{C}$ ), and Sigma-phase formation, due to thermal aging, at the highest test temperatures. No evidence was found that would preclude testing of sodium-bonded, single-phase, uranium-plutonium carbide fuel in a fast flux at lineal power ratings of  $\sim 30\text{ kW/ft}$  to burnups of  $10$  to  $12\text{ at.}\%$ .

## I. INTRODUCTION

Uranium-plutonium carbide is an attractive fuel material for Liquid Metal Fast Breeder Reactor (LMFBR) applications, partly because of its high fissile atom density and thermal conductivity. The interposition of a high conductivity link, such as sodium, between fuel and cladding provides an interesting complement to the high thermal conductivity of the fuel, because the sodium bond is expected to allow operation of fuel pins at  $\approx 30$  to  $40\text{ kW/ft}$  while maintaining relatively low fuel centerline temperatures ( $\approx 1250$  to  $1400^\circ\text{C}$ ).<sup>1,2</sup> By permitting large fuel-clad gaps (as compared to gas-bonded pins), sodium-bonding offers the further potential of high burnup without fuel-clad mechanical interaction. Obvious potential detriments to the concept include: fuel-bond-clad chemical interactions, thermal stress-induced fuel pellet

cracking, bond instability at high heat flux, and whatever safety considerations may arise from bond loss at full power, or from the response of the highly conductive fuel pin to severe overpower conditions. The most fundamental of these potential detriments appears to be chemical interactions, for without favorable equilibrium and/or kinetic conditions in the fuel-sodium-clad system at operating temperatures, the other effects are academic.

To resolve some of the uncertainties associated with the use of sodium-bonded carbides, an experimental program was initiated at the Los Alamos Scientific Laboratory (LASL) ultimately to include: out-of-pile compatibility tests, sodium-bond heat transfer studies, thermal- and fast-spectrum, steady-state irradiations, and transient overpower irradiations. The initial scope of the investigations was determined by (1) the desire by the Division of Reactor Development and Technology that well-known

engineering materials, specifically Type 316 stainless steel, be given prime consideration as cladding candidates,<sup>3</sup> (2) earlier, out-of-pile compatibility test results that suggested that the least fuel-sodium-stainless steel clad interaction might be obtained using carbides with a metal-to-carbon ratio near unity,<sup>4,5</sup> and (3) the fact that LASL could produce essentially single-phase, solid solution carbide material at low oxygen and nitrogen levels.<sup>6</sup> (This material is characterized as single phase, rather than as monocarbide, because structures free from both higher carbides and metal have been obtained at a total anion-to-cation ratio of  $0.97 \pm 0.01$ .) Because of these circumstances, experimentation centered on single-phase solid solution carbide, sodium-bonded to Type 316 stainless steel.

Out-of-pile compatibility studies of this system showed that carbon usually was not transferred in detectable amounts from fuel to the cladding at  $750^{\circ}\text{C}$  for times up to 8000 h.<sup>7</sup> When carbon transport occurred, experimental evidence and thermodynamic calculations indicated that oxygen in the bonding sodium was most likely involved. Fuel pellet surface structures were not altered by contact with low-oxygen sodium, although limited fuel-stainless steel end cap interaction was observed after 8000 h. Compatibility tests were also conducted with hyperstoichiometric multiphase carbide and resulted in depletion of the dicarbide and sesquicarbide phases from the fuel, attack of pellet surfaces by sodium, and carburization of the cladding. Test results were in agreement with reported observations. Carbides containing uncombined uranium and plutonium were not investigated.

Thermal neutron spectrum irradiations of solid solution carbide fuel were undertaken to determine whether fuel, cladding, and sodium would remain mutually compatible at surface burnups of 10 to 12 at.%. While fast spectrum irradiations are preferred to produce the power densities and radial temperature gradients anticipated in LMFBFR's, thermal irradiations appeared useful here because the fuel regions of prime interest (those in contact with sodium) for compatibility studies could be maintained at realistic temperatures. Further, the time required to reach 10 to 12 at.% surface burnup in the available thermal flux was attractive ( $\approx 9$  months), provided the uranium fraction of the carbide fuel was fully enriched in  $^{235}\text{U}$ . Because the out-of-pile tests had shown single-phase fuel to be more nearly inert than fuel containing small amounts of higher carbides, initial irradiations employed single-phase fuel.

## II. EXPERIMENT DESCRIPTION AND OPERATION

Irradiation experiments were conducted at LASL's Omega West Reactor (OWR),<sup>8</sup> a 6 MW MTR-type facility,

in "environmental cells" installed semipermanently in the reactor core. To accommodate the two cells used for these experiments, dummy fuel elements of the type shown in Fig. 1 were installed in the OWR core positions marked 4D and 4F in Fig. 2. Principal features of the cells were: (1) a heat removal and temperature control system consisting of a natural convection sodium loop, electrical heaters, and a variable conductivity heat leak, and (2) a sweep gas system for the rapid detection of leaking fuel capsules. An earlier report<sup>9</sup> describes the cells and their operation in connection with their original purpose of irradiating liquid plutonium alloy fuels. Minor design modifications have been made since.<sup>10</sup>

Figure 3 illustrates the in-core section of a cell with an experimental insert in place. The outside diameter of the cell was 2 in. and its overall length was 22 ft. At the lower end of the cell were the 13-in.-long, electrically heated sodium loop and the variable conductivity heat leak. The concentric legs of the sodium loop were separated by an argon-filled, stainless steel flow divider. The main resistance heaters were wound on the inner surface of the flow divider. Above the insulated flow divider was another heater-wound section that was used at startup to ensure melting of sodium downward from the free surface. The heat leak annulus was formed by the primary sodium container and the cell outer tube. The upper quarter of the annulus was 0.012 in. thick and the remainder was 0.020 in. thick. Thermal conductivity of the annulus was altered by changing the composition of the helium-nitrogen gas mixture flowing through it. Helium, at 10 psig, was used as the cover gas over the sodium in the cell. Three stainless steel-sheathed, chromel-alumel thermocouples were placed in the outer section of the sodium loop. Their junctions were positioned at the top and base

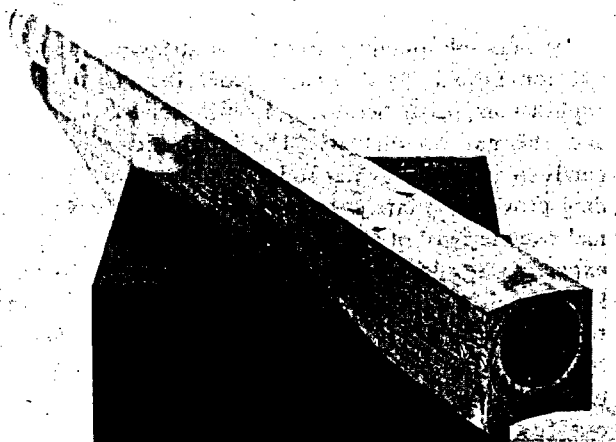


Fig. 1.  
OWR dummy fuel element viewed from top.

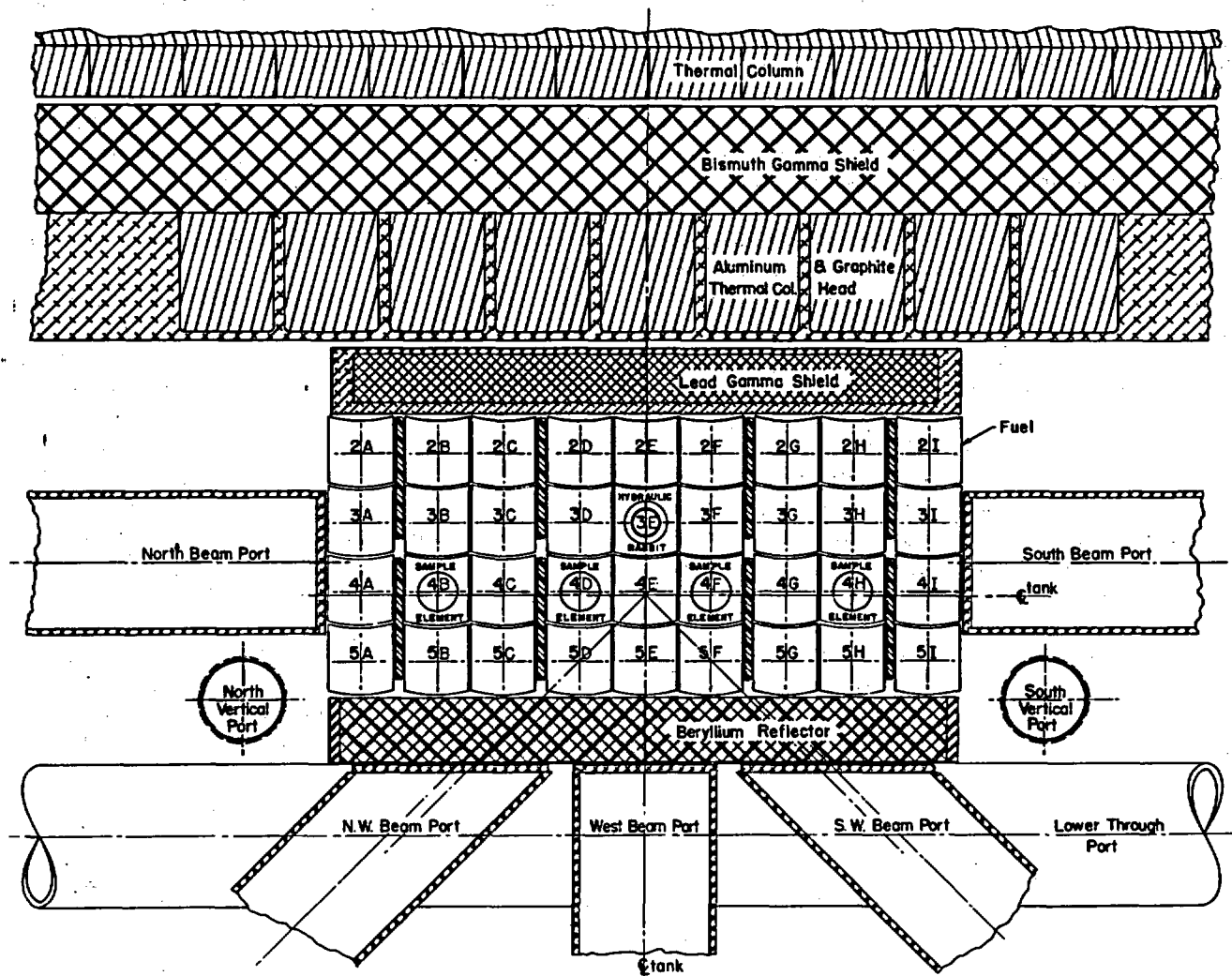


Fig. 2.  
OWR core layout.

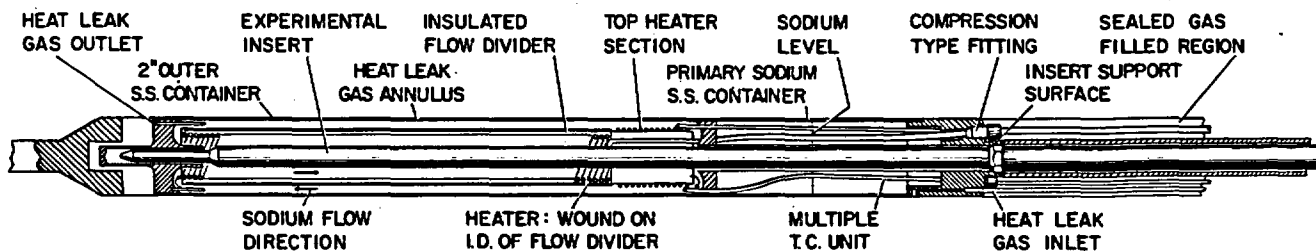


Fig. 3.  
In-core portion of thermal neutron irradiation experiment.

of the section, and adjacent to the transition in the heat-leak-gap thickness. A fourth thermocouple in the outer section of the loop was movable over the length of the section and was used to determine the axial temperature distribution in the sodium.

The experimental insert, occupying the central portion of the cell (Fig. 3), consisted of fuel pins and thermocouples sodium-bonded to an 18-in.-long, 0.60-in.-diam stainless steel secondary container. The secondary container was attached to a 26.5-ft.-long tubular extension, and the entire insert was installed in the cell as a unit. During operation, sodium in the annulus between the experimental insert and the flow divider was heated by the fuel in the insert and by the heaters wound onto the inside of the flow divider. Sodium rose in this annulus and then descended into the annulus between the flow divider and the heat leak wall, transferring heat through the heat leak gas annulus to the reactor cooling water. A helium purge was directed through the volume above the sodium level in the insert and was exhausted from the experiment through a molecular sieve, which was monitored continuously for fission product gases.

The three carbide-fueled inserts, OWREX-14, -15, and -16, that were irradiated in the OWR were identical except in fuel capsule end cap design and thermocouple placement. The fuel was composed of 0.265-in.-diam by 0.250-in.-thick (nominal) pellets of uranium-plutonium

carbide, fully enriched in  $^{235}\text{U}$ . Chemical and isotopic analyses and immersion densities for the various fuel batches used are shown in Tables I, II, and III, and representative microstructures are shown in Fig. 4. Various fuel batches contained a second phase that was plutonium- and silicon-rich and uranium- and carbon-poor with respect to the matrix, and that also contained small amounts of metallic contaminants. This phase comprised  $<0.5$  vol% of the fuel and appeared as small, white inclusions located principally at triple points and pores (Fig. 4b).

Fuel encapsulations were performed in inert-gas gloveboxes equipped with recirculators that maintained water vapor, oxygen, and nitrogen levels at  $\leq 3$  ppm each in the circulating helium. Liquid sodium was supplied directly into one of the boxes from a cold-trapped, forced-convection loop. At the time of encapsulation, this sodium contained oxygen and carbon at levels of 10 to 15 ppm each. Detailed descriptions of the glovebox system and of the encapsulating, bonding, and nondestructive testing procedures for individual fuel capsules have been reported.<sup>11</sup>

Each experimental insert contained two solution-annealed, Type 316 stainless steel fuel capsules, each 2.5 in. long and 0.300-in. diam with a 0.010-in. wall. Each capsule contained three fuel pellets, a stainless steel insulator pellet to separate the fuel from the capsule lower

TABLE I  
CHEMICAL COMPOSITION AND DENSITY OF (U,Pu)C  
FOR THERMAL IRRADIATION EXPERIMENTS

	Batch No.					
	HNL -8-8-1	-8-8-2	-8-16-1	-8-18-1	-8-18-2	-8-62-1
Experiment No.	16	16	14	16	15	15,16
Immersion density: $\text{g}/\text{cm}^3$	12.95	12.98	12.94	12.78	12.98	12.76
Percent theoretical density	96.2	96.4	96.1	95.0	96.4	94.8
Uranium <sup>a</sup>	76.4	76.6	76.5	76.5	76.4	75.3
Plutonium <sup>a</sup>	18.39	18.36	18.73	18.75	18.47	19.67
Carbon <sup>a</sup>	4.72	4.66	4.72	4.73	4.63	4.65
Nitrogen <sup>b</sup>	310	305	270	305	340	225
Oxygen <sup>b,c</sup>	240	360	590	370	320	420
	460	510	830	380	350	340
	510	760		400	640	360

<sup>a</sup>Expressed as wt%.

<sup>b</sup>Expressed as ppm.

<sup>c</sup>Duplicate or triplicate samples.

**TABLE II**  
**ISOTOPIC CONTENT OF U AND Pu IN FUEL**  
**FOR THERMAL IRRADIATION EXPERIMENTS<sup>a</sup>**

Isotope	Batch No.					
	HNL -8-8-1	-8-8-2	-8-16-2	-8-18-1	-8-18-2	-8-62-1
<sup>238</sup> Pu	<0.022	<0.022	<0.010	<0.08	<0.018	
<sup>239</sup> Pu	94.95	94.44	94.45	94.43	94.44	94.27
<sup>240</sup> Pu	5.25	5.26	5.25	5.26	5.26	5.38
<sup>241</sup> Pu	0.281	0.282	0.281	0.283	0.282	0.331
<sup>242</sup> Pu	0.015	0.014	0.015	0.024	0.016	0.017
<sup>244</sup> Pu	<0.0005	<0.0005	<0.0005	<0.0005	<0.0005	<0.0005
<sup>233</sup> U	<0.0005	<0.0005	<0.0005	<0.0005	<0.0005	<0.0005
<sup>234</sup> U	0.940	0.926	0.930	0.940	0.945	0.936
<sup>235</sup> U	92.75	91.22	91.80	92.77	92.98	92.07
<sup>236</sup> U	0.241	0.236	0.240	0.241	0.240	0.237
<sup>238</sup> U	6.07	7.62	7.03	6.05	5.83	6.76

<sup>a</sup> Compositions are in at. %.

closure weld, ~0.3 g sodium, and helium cover gas at one atmospheric pressure. The capsules were stacked end-on-end in the secondary container and were centered in the secondary container by thin stainless steel disks at the top and base of each capsule. Each insert contained eight 0.031-in.-diam thermocouples that were passed through holes in the centering disks and were wired to the fuel capsules. Figure 5 shows a fuel capsule schematically, and Fig. 6 illustrates the assembly method. OWREX-15 and -16 end caps were drawn from sheet stock and were machined to the finished diameter and height.

Procedures for insert assembly and nondestructive testing were developed for an earlier fuel irradiation program and have been reported.<sup>9</sup> Experiment control and alarm circuitry descriptions, operating procedures, and cell performance are also included in Ref. 9.

Gamma and fission heating in the three experiments were measured as follows. Before the start of the carbide experiments, an insert containing no fuel was placed in one cell. With pure nitrogen flowing in the heat leak annulus and with the reactor shut down, the cell was heated electrically and the average temperature drop across the heat leak annulus was measured. The reactor was brought to 6 MW and the cell electrical power was adjusted to maintain the same average temperature drop across the heat leak annulus. The 3-kW difference in electrical power requirement between the two experiments was attributed to gamma heating of the cell and

insert. The dummy insert was replaced with a fueled insert and, with the reactor operating at 6 MW, the same temperature drop was established across the heat leak annulus. The difference in electrical power required by the dummy and fueled inserts amounted to 2.8 kW and was attributed to fission heating in the fuel. Measurements of fission heating in the three experiments agreed within 5% and were equivalent to an average linear heat rating of  $22 \pm 1$  kW/ft. Based on postirradiation axial gamma scans<sup>12</sup> of the experiments, the lower capsule of each experiment generated ~8% less power than did the upper one.

Neutron fluxes through the cell and insert were calculated using a one-dimensional transport code<sup>13</sup> and Hansen-Roach 16-group cross sections;<sup>14</sup> results for the thermal flux component are shown in Fig. 7. Relative radial power distribution in the fuel at the beginning of life was also calculated and was normalized to the measured fission heating value, yielding an average specific power of 170 W/g fuel, a maximum of 670 W/g in the outer 0.001 in. of fuel, and a minimum of 50 W/g at the center (Fig. 8). Although this distribution was not confirmed experimentally, prior experience with one-dimensional predictions for OWR-irradiated fuels has shown good agreement between calculated and radiochemically determined distributions.<sup>9</sup>

Under normal circumstances, the OWR operated at 6 MW for 120 h, Monday through Friday. As a result, the

TABLE III

SPECTROCHEMICAL ANALYSIS OF (U,Pu)C  
FOR THERMAL IRRADIATION EXPERIMENTS

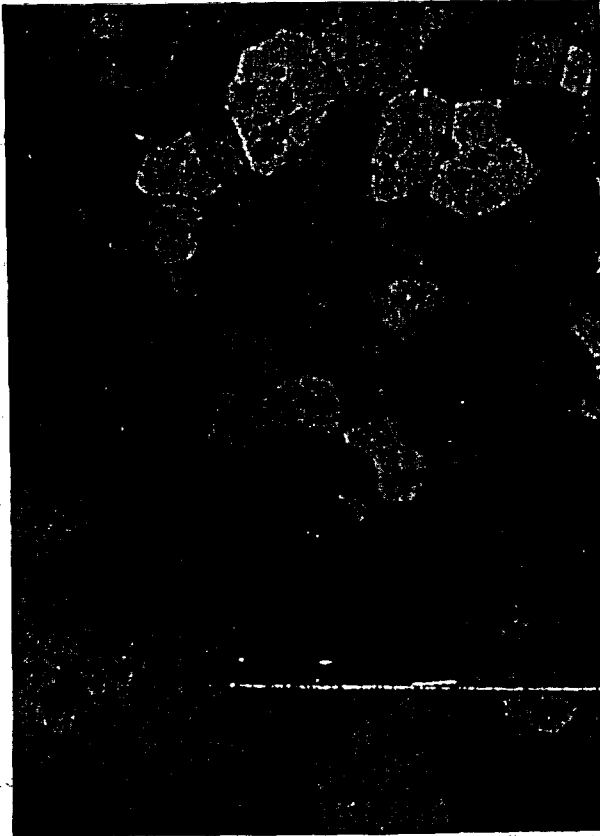
Element	Concentration (ppm)	
	HNL-8-16-2	HNL-8-62-1
Li	< 1	< 2
Be	< 1	< 1
Na	2	< 5
Mg	< 5	< 5
Al	< 10	< 10
Si	35	< 5
P	< 100	< 250
Ca	< 5	< 5
Ti	< 50	
V	5	< 5
Cr	20	< 10
Mn	< 5	< 5
Fe	95	15
Co	< 5	< 5
Ni	10	< 10
Cu	15	< 2
Zn	< 10	20
Sr	< 10	< 10
Zr	< 100	< 100
Nb	< 100	< 100
Mo	10	25
Cd	< 10	< 10
Sn	< 5	< 5
Ta	< 1000	< 1000
W	< 10	< 10
Pb	< 10	10
Bi	< 2	< 2

experiments were heated by fission for 62 to 65% of the total time at elevated temperature and by resistance heaters for the remainder. The change from nuclear to electrical heating affected axial as well as radial temperature gradients in the experiments. Differences in the axial gradient resulted from the fact that when the reactor was not operating, heat was supplied over the entire length of the insulated flow baffle, whereas during reactor operation, approximately half the required heat was generated within the two fuel samples. Axial temperature gradients were measured over  $\frac{1}{4}$ - or  $\frac{1}{2}$ -in.-long, fuel-containing segments of each capsule in each experiment. At a reactor power of 6 MW, temperature gradients over  $\frac{1}{2}$ -in. lengths were 47, 50, 51°C, and over  $\frac{1}{4}$ -in. lengths were 23, 23, and -19°C. Excluding the negative gradient, which probably resulted from one thermocouple breaking away from

a capsule, the average axial gradient was 96°C/in. fuel. With the reactor shut down and the resistance heaters supplying essentially all the heat, the axial temperature gradient varied from 6 to 8°C/in. fuel, approximately one-fourth that observed during reactor operation. Table IV shows the difference in fuel capsule temperature ranges for the three experiments during reactor operation and after shutdown. The limits shown in Table IV reflect variations in reactor power, cooling water temperature, peak flux (axial) location, and positions of thermocouples used for temperature control in the three experiments. The smaller temperature variations experienced by the top capsule of each experiment resulted from the use of that capsule for temperature control during shutdown.

Additional temperature variations occurred during normal reactor startup and shutdown, and during reactor scrams. With the reactor shut down, pure nitrogen was directed into the heat leak annulus to minimize the requirement for electrical heat and, thereby, extend heater lifetime. During reactor ascent to power, electrical heating requirements decreased, reaching zero at a reactor power of 3 MW. A change in heat leak gas composition (conductivity) was necessary to avoid overheating during the experiments. A mixture of 75 vol% helium and 25 vol% nitrogen was introduced into the heat leak annulus at a reactor power of 3 MW and, after a short delay, the ascent to full reactor power was resumed. Both temperature traces of Fig. 9a and the higher temperature trace of Fig. 9b show the response of fuel-containing capsule sections as the reactor was brought to power. Temperatures increased until, at 3 MW, the more conductive heat leak gas was introduced, after which fuel temperatures decreased rapidly. This trend was reversed by the electrical heaters. As reactor power was increased above 3 MW, temperatures increased gradually, exceeding normal operating ranges for a few minutes. The low-temperature trace of Fig. 9b shows the response of a sodium meniscus region; here the temperature rose before introduction of the helium-nitrogen mixture, dropped rapidly until the heaters became effective, and then dropped more slowly as reactor power increased and less electrical power was required to maintain the desired fuel temperatures. During descent from operating power (Figs. 9c and 9d), the fueled portions of the capsules cooled until, at 3 MW, pure nitrogen was reintroduced into the heat leak annulus. As the gas reached the annulus, there was a rapid temperature rise counteracted at first by reduced electrical heat and later by the continuing reduction in reactor power. The sodium meniscus trace of Fig. 9d again moved in opposition to the fuel traces as electrical heat was substituted for fission heat.

Temperature traces recorded during a scram and subsequent startup are shown in Fig. 10. Nitrogen was substituted for the helium-nitrogen mixture as reactor power



a. Fuel microstructure free from additional phases.



b. Fuel microstructure exhibiting small white inclusions of plutonium- and silicon-rich material.

Fig. 4.

Representative microstructure of fuel before irradiation.

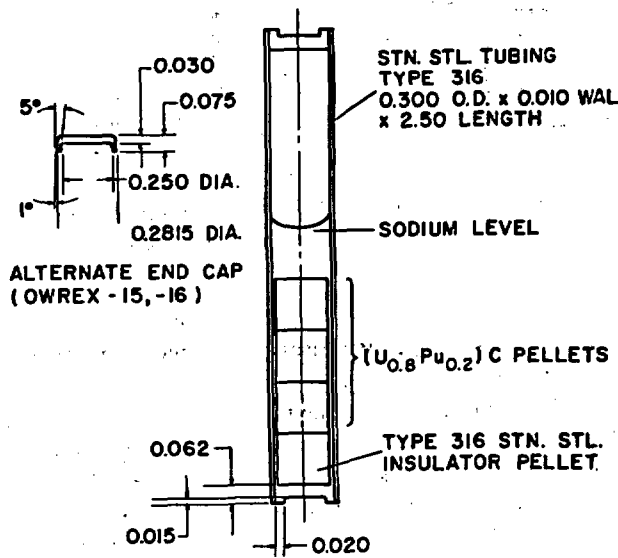


Fig. 5.

OWREX fuel capsule and alternate end cap.

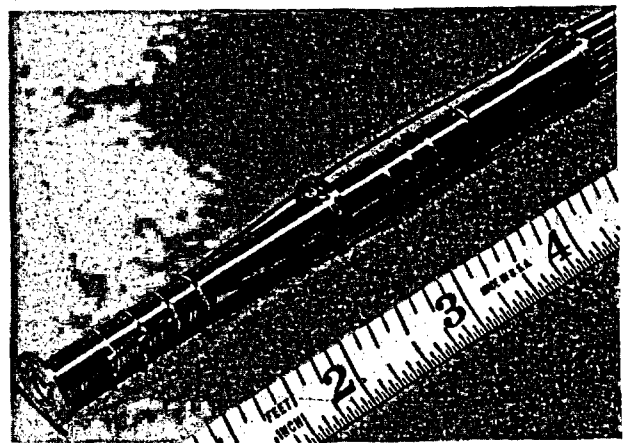


Fig. 6.

Fuel capsules before insertion in secondary container.

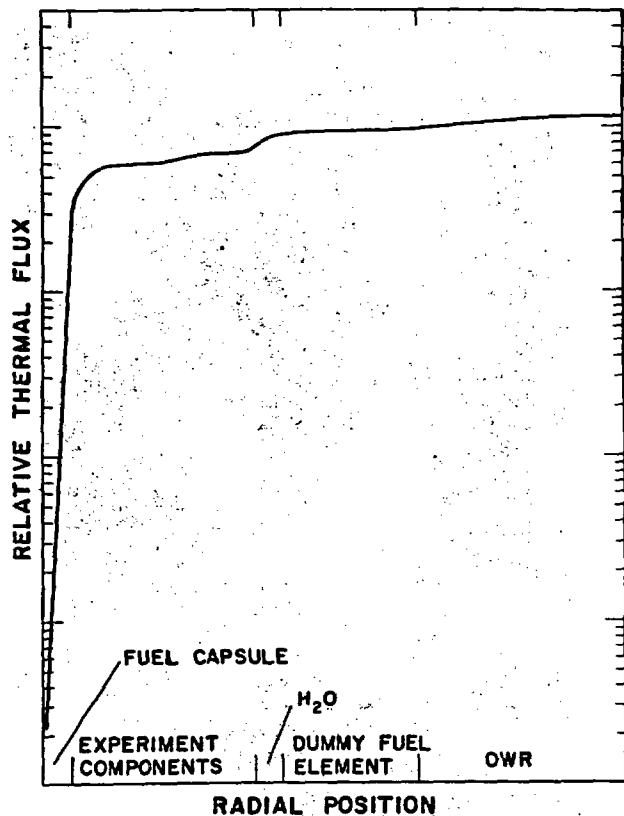


Fig. 7.

Predicted thermal flux distribution for  $(^{235}\text{U}_{0.8}\text{Pu}_{0.2})\text{C}$  irradiations.

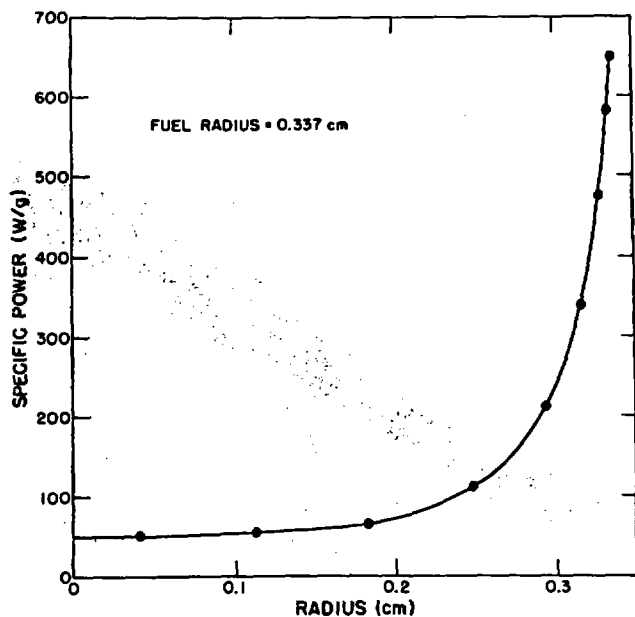


Fig. 8.

Predicted radial power distribution in  $(^{235}\text{U}_{0.8}\text{Pu}_{0.2})\text{C}$  at reactor power of 6 MW.

TABLE IV  
NOMINAL OPERATING TEMPERATURES OF SODIUM-BONDED (U,Pu)C-CONTAINING CAPSULES

Position	Temperature, °C	
	At Power	Shutdown
Lower capsule, adjacent to:		
Base of fuel stack	570 ± 10	577 ± 5
Top of fuel stack	640 ± 10	581 ± 5
Na meniscus	535 ± 15	581 ± 6
Upper capsule, adjacent to:		
Base of fuel stack	600 ± 5	596 ± 5
Top of fuel stack	675 ± 8	601 ± 5
Na meniscus	548 ± 10	603 ± 5

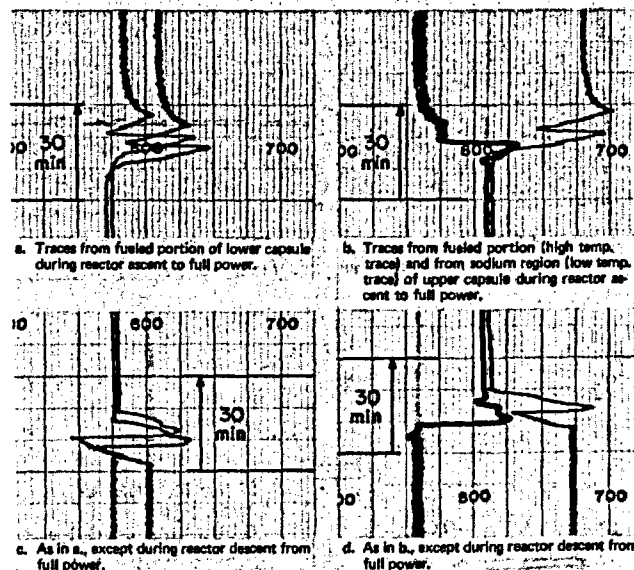


Fig. 9.

Response of OWREX-16 fuel capsule thermocouples to normal reactor startup and shutdown.

decreased through 3 MW, but the rapid decrease in fission heating led to large decreases in capsule temperatures before the electrical heaters became effective.

Radial temperature gradients through fuel, bond, and cladding at the beginning of life were approximated using the specific power values shown in Fig. 8. Heat was assumed to flow only in the radial direction, and fuel and clad were assumed to be coaxial. The temperature drop associated with the outward flow of heat through a hollow cylinder can be expressed as<sup>15</sup>

$$t_i - t_o = \frac{q}{2\pi k \ell} \ln \frac{r_o}{r_i}$$

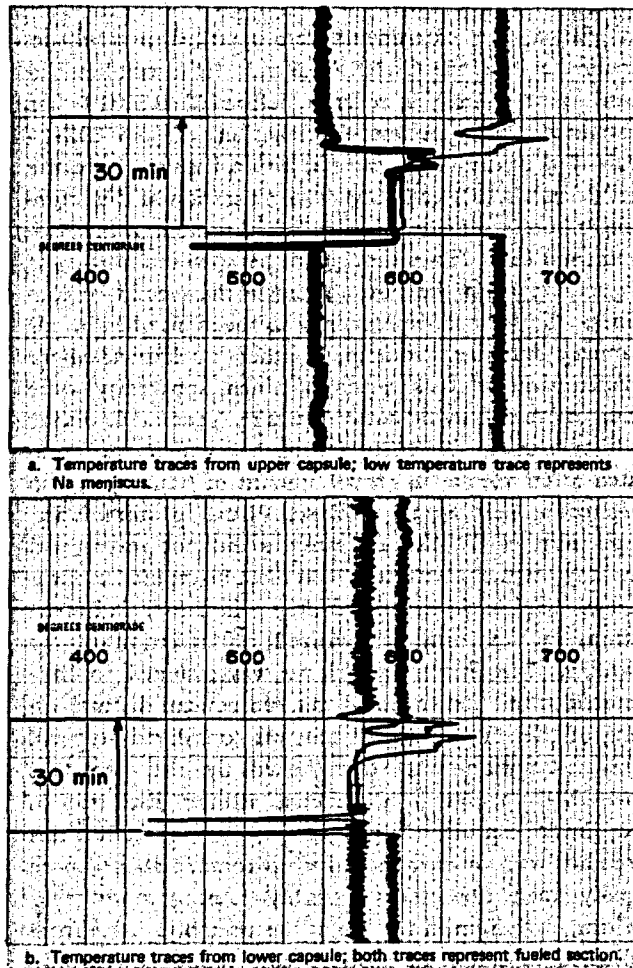


Fig. 10.

Response of OWREX-16 fuel capsule thermocouples to reactor scram and subsequent normal ascent to power.

where  $r_o$  and  $r_i$  are the outer and inner radii,  $\ell$  is the axial dimension,  $k$  is the conductivity, and  $q$  is the rate of heat flow. For uniform heat generation in a hollow cylinder, the temperature drop associated with the outward flow of heat is

$$t'_i - t'_o = \frac{Q}{2\pi k \ell} \left( \frac{1}{2} - \frac{r_i^2}{r_o^2 - r_i^2} \ln \frac{r_o}{r_i} \right),$$

where  $Q$  is the total heat generation rate within the volume. The temperature drop associated with the flow of heat through a cylindrical segment, and with the generation and flow of heat within the same segment, is the sum of the two expressions

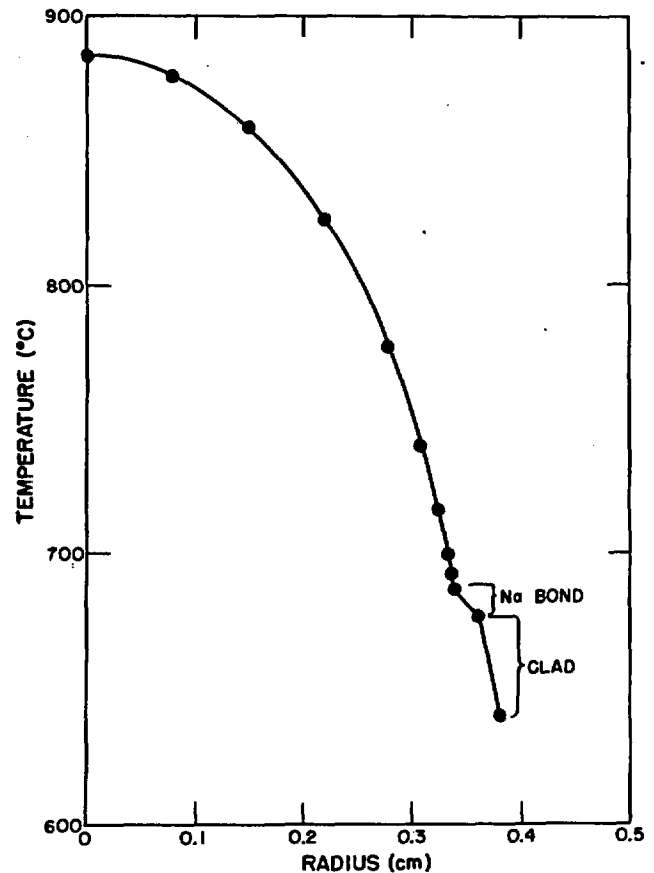


Fig. 11.

Beginning-of-life radial temperature distribution in (U,Pu)C fuel capsule, neglecting end effects.

$$t''_i - t''_o = \frac{1}{2\pi k \ell} \left[ q \ln \frac{r_o}{r_i} + Q \left( \frac{1}{2} - \frac{r^2}{r_o^2 - r_i^2} \ln \frac{r_o}{r_i} \right) \right].$$

This expression was evaluated for each volume segment used in the one-dimensional, neutron-transport calculation, after setting the clad outside surface temperature and assuming the various conductivities to be independent of temperature over the temperature range of interest. The results are shown in Fig. 11; temperature drops through cladding, sodium, and fuel were  $\sim 37$ , 10, and  $200^\circ\text{C}$ , respectively, for a cladding outside surface temperature of  $640^\circ\text{C}$ . The range of fuel operating temperatures shown in Table V was based on these predicted radial gradients and on measured cladding temperatures. Because of thermal stress-induced fuel cracking and subsequent ingress of sodium, fuel centerline temperatures probably were lower than the estimates in Table V.

TABLE V

FUEL NOMINAL OPERATING TEMPERATURES<sup>a</sup>

Surface temperature (°C)	
minimum	610
maximum	730
Centerline temperature (°C)	
minimum	810
maximum	930

<sup>a</sup>At start-of-life, assuming sound fuel pellets concentric with cladding.

## III. RESULTS

## A. General

Upon completion of an irradiation, the portion of the insert containing the fuel capsules was separated from the remainder of the insert, radiographed, and scanned<sup>12</sup> to determine the axial distribution of gamma activity and the relative distributions of <sup>137</sup>Cs, <sup>95</sup>Zr-<sup>95</sup>Nb, <sup>103</sup>Ru, <sup>140</sup>Ba-<sup>140</sup>La, and <sup>131</sup>I. The fuel capsules were dissected, and selected portions were autoradiographed and examined by optical microscopy and electron beam microprobe techniques. Because of the large radial variation in fuel power density, measurements of fission gas release and fuel and clad swelling were not made.

A brief operating history of the experiments is shown in Table VI. Calculated burnups appearing in the table were based on fission events and did not account for fissile uranium and plutonium removed by other processes (principally radiative capture). Taking the latter into account, a surface burnup of 15.9 at.% was calculated for OWREX-16.<sup>16</sup> Also, the tabulated burnups were derived from (1) the measured initial fission heat rate, (2) the calculated initial radial power distribution, and (3) the OWR operating histories. To account for the removal of fissionable material, particularly from the outer, high-burnup region of the fuel, as the irradiations progressed, a time-dependent burnup calculation was performed for OWREX-16. The results showed the maximum burnup in Table VI to be 0.1 at.% high, which is a smaller error than that arising from the uncertainty in the measured heat generation rate. Over the experiment lifetime, the ratio of edge-to-center fission rate decreased from ~12:1 to 10:1.

The first and third assemblies completed planned irradiations without fuel capsule failure; the second assembly was removed a week earlier than planned after a fission

gas release. The experiments were operated in rapid succession so that the OWREX-15 and -16 assemblies had been inserted in the reactor before OWREX-14 was examined. The posttest examination of OWREX-14 showed that the lower capsule had collapsed above the fuel (Figs. 12,13), probably during insertion of the room-temperature assembly into the 250°C sodium of the environmental cell. This is thought to have caused melting of the sodium from the base upward in the secondary container. All previous experiments had been installed in this manner, but they contained either thicker-walled or smaller-diameter fuel capsules, which apparently were able to resist hydrostatic pressure generated during sodium melting. OWREX-15 (Fig. 14), which was terminated after release of a small amount of fission gas, also suffered a fuel capsule collapse. Visual, postirradiation inspection of OWREX-15 capsules did not reveal clad cracking or fuel penetration, and metallographic examination of clad sections showed only minor fuel-clad interaction, in the form of localized carburization of the cladding. The fission gas release was assumed to have resulted from the crushing and subsequent thermal cycling of the lower capsule, and was considered atypical. This assumption was strengthened by the fact that OWREX-16 operated, as planned, without distortion of the lower capsule (Figs. 15,16). Coincidentally, this assembly was lowered into the environmental cell more rapidly than the others, possibly causing more rapid melting of sodium in the top of the assembly. Aside from collapsed capsules, the posttest radiographs showed only increasing fuel cracking and spalling with increasing time (Figs. 12, 13, and 15).

Upon visual examination, all capsules appeared frosted or lightly etched in the region of high heat flux and discolored over the remaining surface area (Figs. 13,16). Light scratching of the capsules removed the discoloration, indicating a surface phenomenon, and subsequent metallographic examination of cladding sections failed to associate a microstructural feature with the discolored surfaces. Because control of oxygen in the secondary bonding sodium was crude at best, the exterior appearance of the capsules was not of primary importance.

## B. Gamma Scanning

The distributions of gross gamma activity and of individual fission products in the fuel capsules were determined by scanning each experiment with a Ge(Li) detector operating in anticoincidence with a large, annular NaI (TI) crystal.<sup>12</sup> Events generated by gamma photons (energy > 100 keV) incident on the detector from a well collimated beam were counted and stored on one channel of a 4096 channel pulse height analyser.<sup>17</sup> The fuel

**TABLE VI**  
**OPERATING HISTORY OF MIXED CARBIDE IRRADIATIONS**

	<u>OWREX-14</u>	<u>OWREX-15</u>	<u>OWREX-16</u>
Startup date	12-8-69	1-12-70	3-30-70
Shutdown date	3-14-70	6-10-70	12-24-70
Total time at elevated temperatures (h)	2343	3559	6719
Total time at power (h)	1454	2308	4198
Computed burnup <sup>a</sup>			
Surface <sup>b</sup>	4.4	7.3	13.0
Average	1.1	1.8	3.2
Estimated peak thermal neutron fluence at cladding (n/cm <sup>2</sup> )	$1 \times 10^{20}$	$1.6 \times 10^{20}$	$3 \times 10^{20}$
Remarks	Completed successfully	Terminated by fission gas release	Completed successfully

<sup>a</sup>Burnup is defined as the percentage of initial fissile atoms removed by fission.

<sup>b</sup>Surface value is the average in the outermost 0.001 in. annulus of fuel.

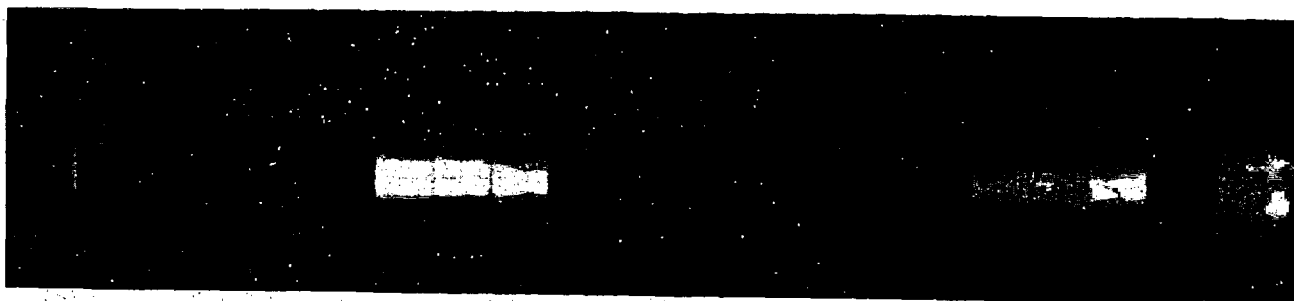


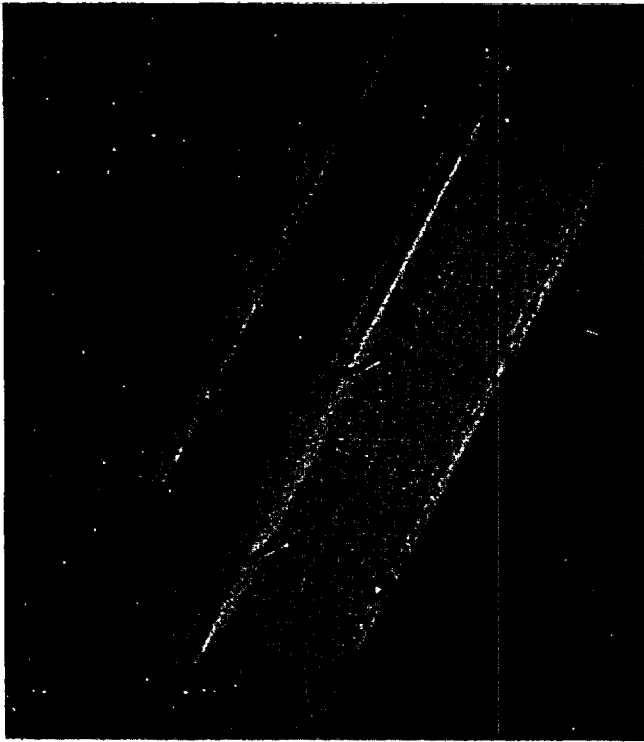
*Fig. 12.*

*A 22-MeV Betatron x-radiograph of OWREX-14 assembly after irradiation (outermost container is an alpha can).*

assembly was moved 0.010 in. and information was accumulated in a second channel. The process was repeated until the region of interest had been inspected. Distributions of specific gamma-emitting fission products were obtained by recording a portion of the gamma-ray spectrum between 70 and 2000 keV at 0.020-in. increments along the length of each experiment, determining areas under pertinent full-energy photopeaks and applying an average background correction.

The postirradiation axial distribution of activities failed to show fission product redistribution, although a 5 to 10% difference in average gross gamma activity (as well

as in individual species gamma activities) was noted between the upper and lower capsule in each experiment. The distribution of gamma activities in the experiments is typified by the results from OWREX-16 (Figs. 17-21). The gross gamma scan of the upper capsule (Fig. 17) showed the following features: the upper end cap and centering disk occupying the region between 17- $\frac{1}{4}$  and 17- $\frac{1}{2}$  in. on the abscissa, fuel occupying the region between 18- $\frac{3}{4}$  and 19- $\frac{1}{2}$  in. and reflecting the relatively high burnup at the top and bottom surfaces of the stack, and the stainless steel insulator pellet, the lower end cap, and the lower centering disk occupying the region



*a. Upper capsule.*



*b. Lower capsule.*

*Fig. 13.*

*Fuel capsules from OWREX-14 after removal from secondary container.*



*Fig. 14.*

*A 22-MeV Betatron x-radiograph of OWREX-15 assembly after irradiation to 7.3 at.% surface burnup.*

between 19- $\frac{1}{2}$  and 19.9 in. This distribution was repeated in the lower capsule, extending from 19.9 to 22.4 in. on the abscissa of Fig. 17. The activity beginning at 22.9 in. was associated with the end plug of the secondary container, from which the fuel capsules were separated at the end of the irradiation.

The distributions of individual fission products (Figs. 18-21) were similar to one another and to the gross

gamma distribution except in regions where stainless steel activation products contributed significantly to the gross gamma distributions (end caps, spacers, and dummy pellets). The  $^{103}\text{Ru}$  plots of Fig. 18 appear to differ from the other single species scans, but this results from changing the ordinate from logarithmic to linear to emphasize the increased burnup at the ends of the stacks. The other

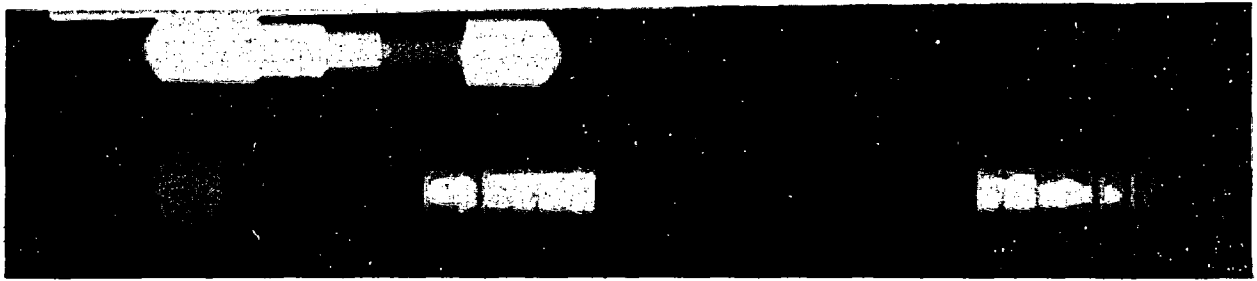
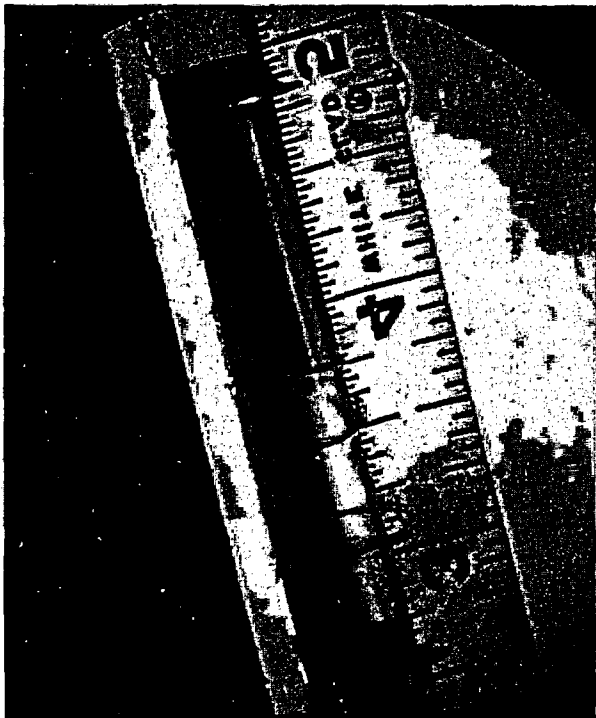
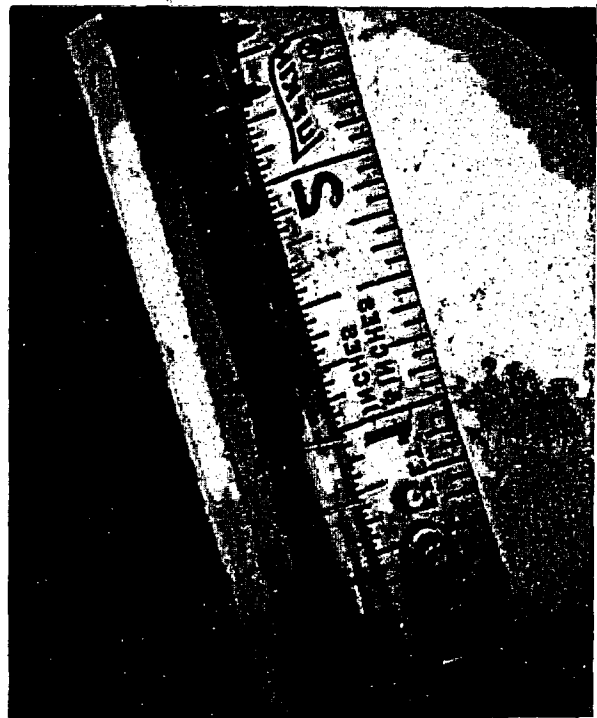


*Fig. 15.*

*A 22-MeV Betatron x-radiograph of OWREX-16 assembly after irradiation to 13 at.% surface burnup. (Object at bottom is a dimensional standard.)*



*a. Upper capsule.*



*b. Lower capsule.*

*Fig. 16.*

*OWREX-16 fuel capsules after removal from secondary container. (Stains near wire ties were caused by sodium-air reaction products.)*

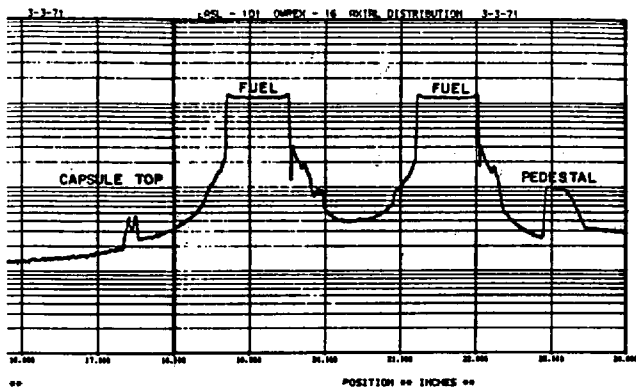


Fig. 17.  
Axial distribution of gamma-emitting species in OWREX-16 assembly ( $E > 100$  keV).

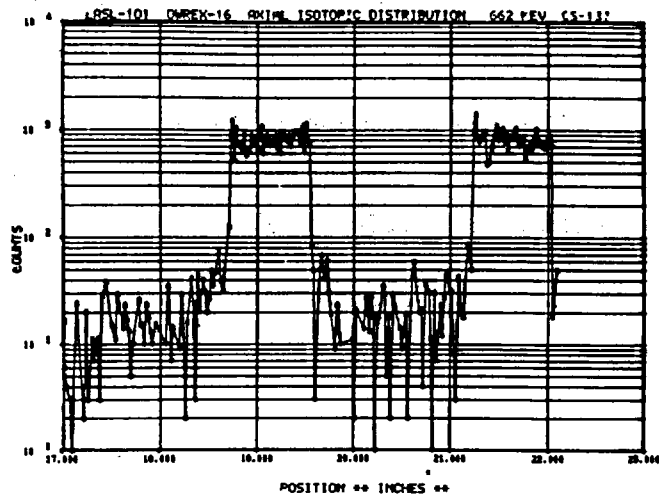


Fig. 19.  
Axial distribution of <sup>137</sup>Cs in the OWREX-16 assembly.

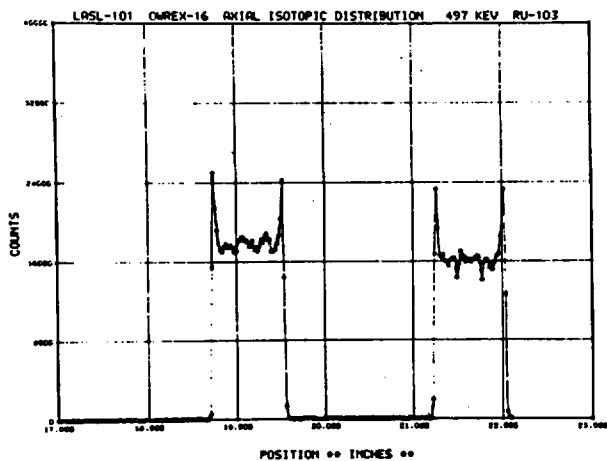


Fig. 18.  
Axial distribution of <sup>103</sup>Ru in the OWREX-16 assembly.

characteristic accentuated in Fig. 18 is the drop in activity corresponding to the fuel pellet-pellet interfaces.

Apart from the fueled regions of the capsules, fission product activity was detected at ~18.5 and 21 in. (Figs. 19, 20, and 21), the regions of the sodium menisci. An additional region of activity was found at 19.8 in., ~¼ in. below the fuel stack in the top capsule, and a similar region of activity was noted in the lower capsule but is not shown in the figures. Because all these regions contained all the fission products for which a search was made, the activities most likely were associated with fuel chips and smaller particles that either sank to the bottom or were suspended at the meniscus.

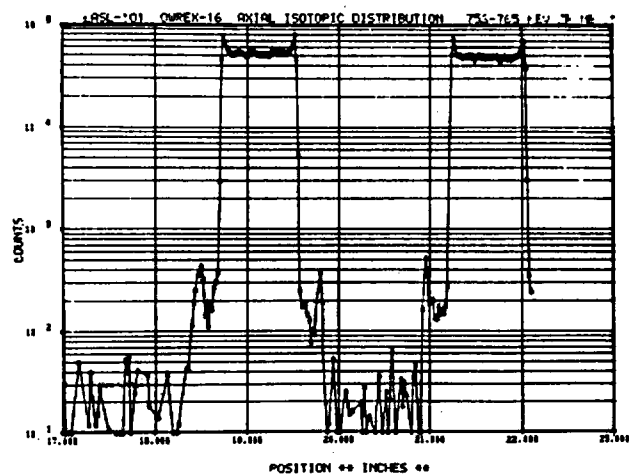


Fig. 20.  
Axial distribution of <sup>95</sup>Zr-<sup>95</sup>Nb in the OWREX-16 assembly.

### C. Destructive Examinations

The upper, or higher temperature capsule from OWREX-14 and -15 and both capsules from OWREX-16 were dissected in argon atmospheres containing < 10 ppm O<sub>2</sub> and < 2 ppm water vapor.<sup>18</sup> Bonding sodium was removed from the fuel capsules by reaction with absolute ethanol. The upper capsule from each experiment was

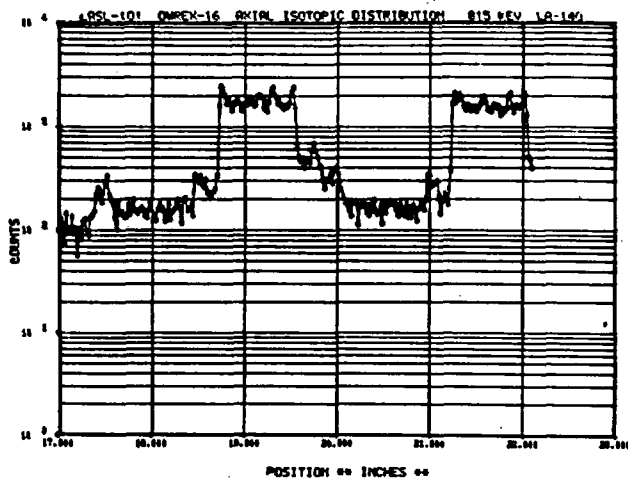


Fig. 21.  
Axial distribution of  $^{140}\text{Ba}$ - $^{140}\text{La}$  in the OWREX-16 assembly.

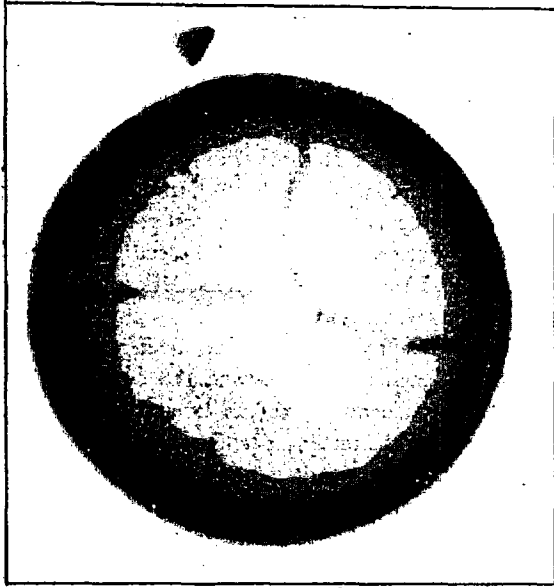
sectioned in an attempt to obtain (1) a transverse specimen of fuel and cladding from the highest temperature region, (2) a longitudinal specimen of fuel and cladding from each sodium-cover gas interface region, and (3) a longitudinal cladding specimen encompassing the remainder of the fuel pellet region. The lower capsule from OWREX-16 was sectioned to obtain a transverse fuel-clad specimen from the cold end. Insulator pellets from the four capsules were sectioned in the longitudinal direction. The sections and their approximate locations in the capsules are listed in Table VII.

1. Autoradiography. Alpha and beta-gamma autoradiographs of each section showed the activities to be distributed nonuniformly along all inner surfaces of the cladding and along the insulator pellet surfaces. The distributions of alpha and beta-gamma activities were similar, indicating that fuel material was present, as opposed to fission products only. No autoradiographic evidence could be found to suggest that fuel or fission products had penetrated into the container alloy. The beta-gamma autoradiograph of transverse fuel-clad Sec. 1B23 from OWREX-16 (Fig. 22a) illustrates the superficial nature of the burnup. The apparent increase in activity at the fuel

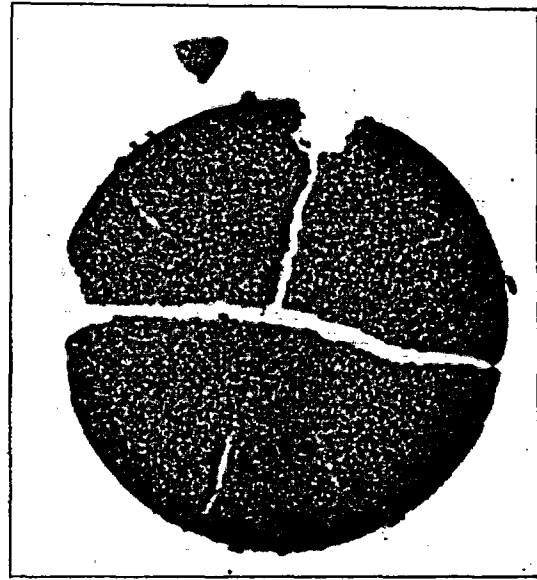
TABLE VII  
SPECIMENS PREPARED FROM OWREX-14, -15, AND -16  
FUEL CAPSULES

Experiment and Capsule	Section Number	Section Type and Location <sup>a</sup>
OWREX-14, Top capsule	OA88	insulator pellet, L
	OA90	clad adjacent to top of fuel stack, T
	OA92	fuel, top of fuel stack, T
	OA91	clad, lower fueled section of capsule, L
	OA89	clad, region of Na meniscus, L
OWREX-15, Top capsule	OA93	fuel, top of fuel stack, T
	OA95	fuel, center of fuel stack and clad adjacent to top of fuel stack, T
	OA94	clad, region of Na meniscus, L
	OA96	clad, lower fueled section of capsule, L
	OA98	insulator pellet, L
OWREX-16, Top capsule	1B23	fuel and clad, top of fuel stack, T
	1B24	clad, region of Na meniscus, L
	1B25	clad, lower fueled section, L
	1B26	insulator pellet, L
OWREX-16, Bottom capsule	1B27	fuel and clad, base of fuel stack, T
	1B28	insulator pellet, L

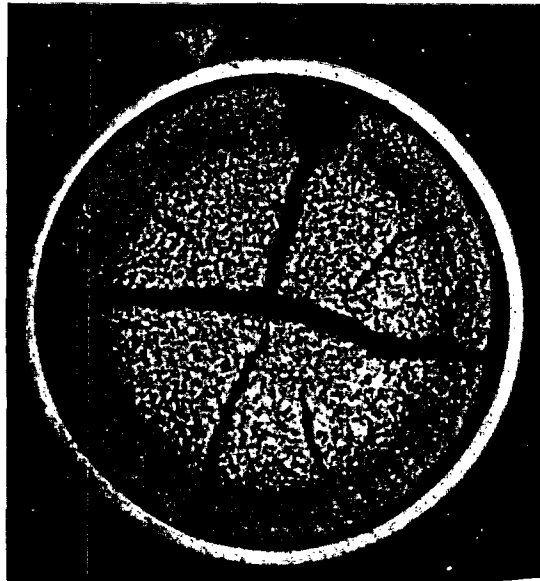
<sup>a</sup> L = longitudinal, T = transverse.



(a)



(b)



(c)

Fig. 22.

*Transverse fuel-clad section from OWREX-16. 10X. (a)  $\beta$ - $\gamma$  autoradiograph; (b)  $\alpha$ -autoradiograph; (c) direct light photograph.*

periphery in the alpha autoradiograph is believed to result from the sensitivity of the film to low energy beta particles originating in this high-burnup region.

**2. Metallography.** Transverse Sec. OA90 from OWREX-14 is shown in Fig. 23 after this portion of the experiment operated for 2340 h at a cladding inner surface temperature of  $\sim 700^\circ\text{C}$ . Isolated regions were found in which the cladding had been penetrated intergranularly and from which surface grains had been removed during polishing (Fig. 23a). Whether this pullout was a result of irradiation or of storage before metallographic examination was not established. In the etched condition the cladding inner surface exhibited heavier-than-average concentrations of precipitates, assumed to be  $M_{23}C_6$ -type carbides, in a few locations (Figs. 23b, 23c), and an additional few white, precipitate-free surface zones (Fig. 23d). Fuel from this section achieved 4.4 at.% burnup but could not be distinguished from control specimens. The longitudinal cladding section (not shown) comprising the remaining fueled portion of the OWREX-14 upper capsule showed inter- and intragranular precipitates and grain pullout along the inner surface. The longitudinal cladding section from the sodium meniscus region showed none of the unusual characteristics of the other cladding sections. The stainless steel insulator pellet, Sec. OA88, on which the carbide fuel had rested is shown in Fig. 23f. Precipitates were visible in the slip planes near the surface, accompanied by a thin, intermittent, precipitate-free layer at the surface. Pullout of surface grains was not observed in this specimen. Because significant fuel-clad interaction was not observed in the higher temperature capsule from OWREX-14, the lower temperature capsule was not examined.

The upper fuel capsule from OWREX-15 was examined destructively after operating for 3650 h at elevated temperature and attaining 7.3 at.% fuel surface burnup. Cladding inner surfaces that operated at  $\sim 700^\circ\text{C}$  showed intermittent inter- and intragranular precipitates (Secs. OA94 and OA96), Figs. 24a and 24b. At other locations in the same sections, the oxalic acid etchant failed to delineate some grain boundaries (Fig. 24c), and overetched others, primarily in the vicinity of triple points. Intragranular precipitates imparted a stippled appearance to the cladding. Repeated polishing and etching revealed the same structures. Because the oxalic acid etchant was specific for carbides, the white grain boundaries apparently were deficient in carbides relative to the remainder of the cladding.

The longitudinal cladding section through the sodium meniscus of the OWREX-15 capsule exhibited intermittent carburization at the lower, or sodium-filled end and random loss of grains, the latter occurring even in the capsule gas space. The stainless steel insulation pellet (Sec.

OA98, Fig. 24d) showed the same features as the insulator pellet from the first irradiation: a surface band free from precipitates and an adjacent band containing a higher-than-average concentration of precipitates.

Two fuel sections from OWREX-15 were examined and appeared to have undergone no significant changes during irradiation (Fig. 25). White inclusions having the appearance and distribution of the plutonium- and silicon-rich inclusions sometimes seen in the as-fabricated fuel (Fig. 4b), were observed in both irradiated sections.

OWREX-16 operated for  $\sim 6700$  h at an elevated temperature and reached a fuel surface burnup of  $\sim 13$  at.%. Both capsules were examined destructively. Fuel-clad sections from the highest temperature portion of the top capsule and from the lowest temperature portion of the bottom capsule are shown in Figs. 26 and 27. The difference in operating temperature between these sections was  $\sim 100^\circ\text{C}$ . The low temperature section appeared unchanged except for cracking of fuel and weeping of sodium reaction products from fuel pores, accounting for the large dark blobs visible in Fig. 26. An annular region of fine cracks, beginning  $\sim 0.010$  in. beneath the fuel surface and extending inward another 0.030 in. was visible in the higher temperature section, Fig. 27. The polished specimen showed no other features.

The etched capsule wall from the colder section is shown in Fig. 28a. The inner surface showed a slight nonuniform precipitate, assumed to be  $M_{23}C_6$ -type carbides. The exterior portions of the wall contained significant grain boundary precipitates, assumed to be  $M_{23}C_6$ -type carbides deriving from poor control of oxygen or carbon levels in the secondary bonding sodium during assembly and operation of the experiment. Etched fuel from the colder section is shown in Figs. 28b and 28c. The only obvious departure in appearance from as-fabricated material was staining caused by the weeping of sodium reaction products. Small light-colored inclusions were observed throughout the fuel and were assumed to be the silicon- and plutonium-rich material found in control samples.

An increase of  $100^\circ\text{C}$  in operating temperature caused a significant change in the postirradiation appearance of the etched cladding, as shown by transverse Sec. 1B23, Fig. 29. The cladding had a stippled appearance throughout, and exhibited heavier grain boundary precipitates along the outside surface than along the inner surface. At intervals along the inner third of the cladding wall, grain boundaries failed to etch, producing the white network visible in Figs. 29a and 29b, and material in the vicinity of some triple points took on a coarse, black appearance. An additional few regions along the inner surface exhibited a thin, white layer and an intergranular phase (Fig. 29c). Repeated polishing and etching of the cladding did not alter its appearance.



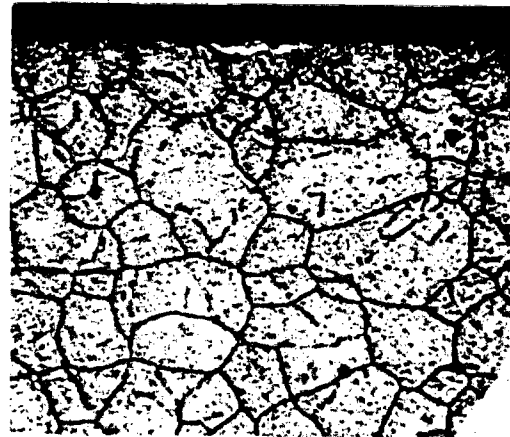
(a)



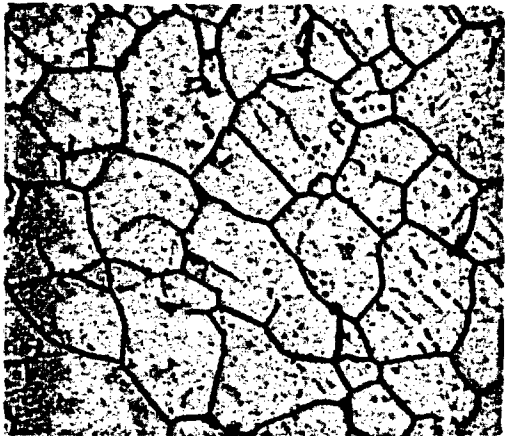
(b)



(c)



(d)



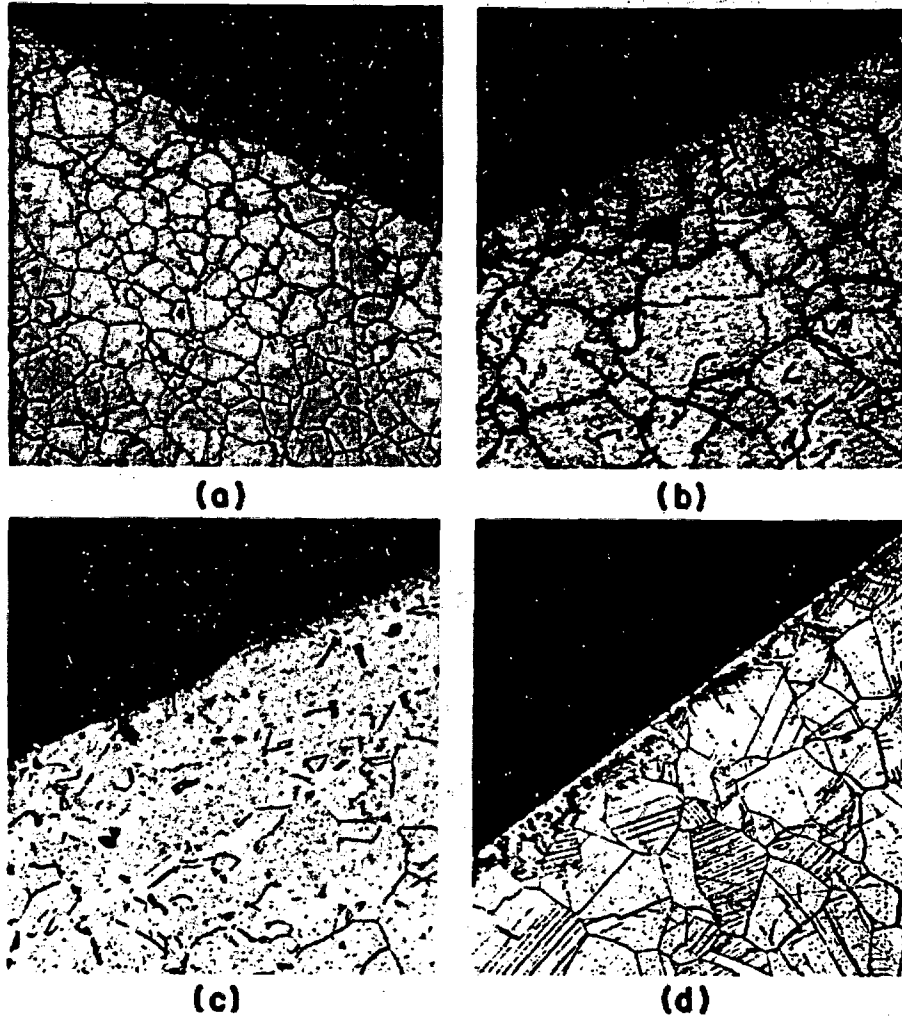
(e)



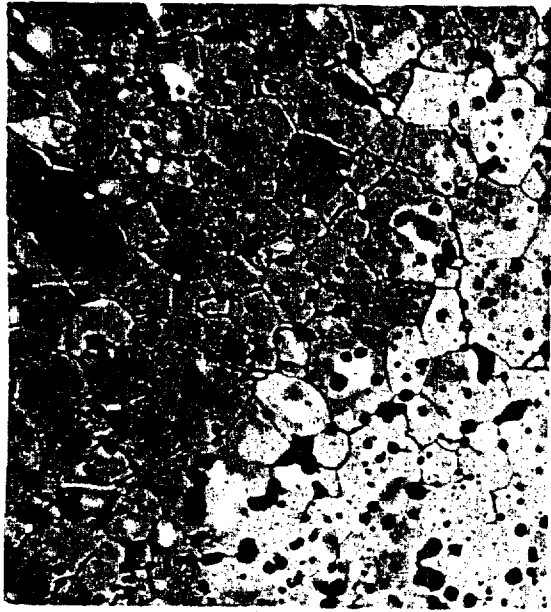
(f)

Fig. 23.

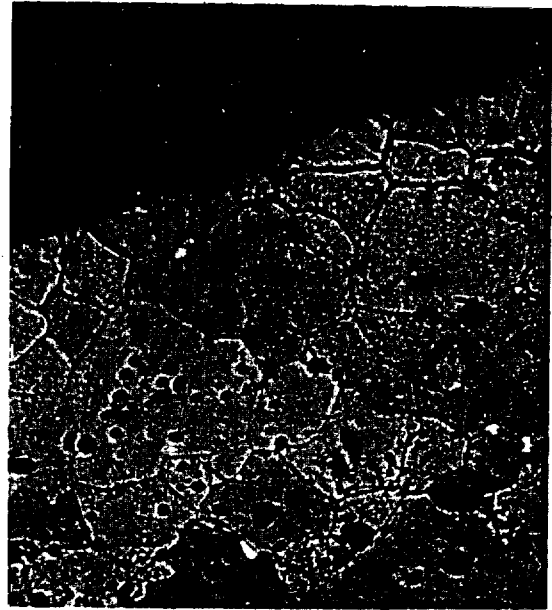
Type 316 stainless steel from OWREX-14 irradiation. (a) Inner surface of transverse cladding specimen OA90, as-polished, 300X, (b, c, d) inner surface of transverse cladding specimen OA90, oxalic acid electrolytic etch, 525X, (e) center of wall from transverse cladding specimen OA90, oxalic acid electrolytic etch, 525X, (f) fuel contact surface of insulator, Sec. OA88, oxalic acid electrolytic etch, 525X.



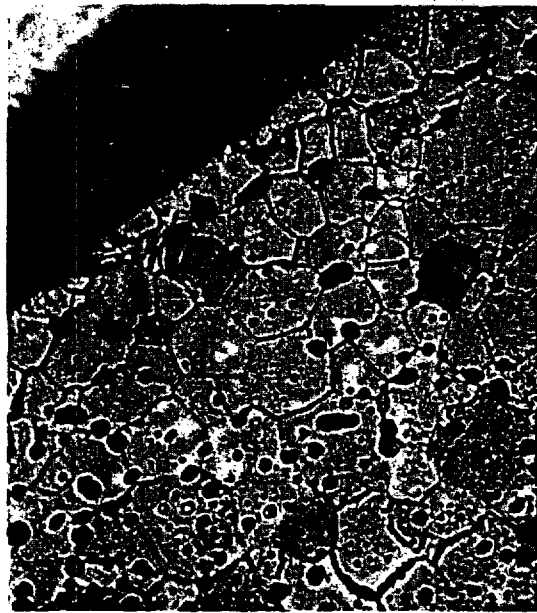
**Fig. 24.**  
*Type 316 stainless steel from OWREX-15 irradiation, oxalic acid electrolytic etch, (a) inner surface of transverse cladding specimen OA94, 300X, (b, c) inner surface of longitudinal cladding specimen OA96 at high temperature end of capsule, 525X, (d) fuel contact surface of insulator pellet, Sec. OA98, 300X.*



(a)



(b)



(c)

Fig. 25.  
OWREX-15 fuel, lactic-acetic-nitric acid etch (2:2:1), 300X, (a) fuel interior from longitudinal Sec. OA93, (b,c) fuel surface from transverse Sec. OA95.

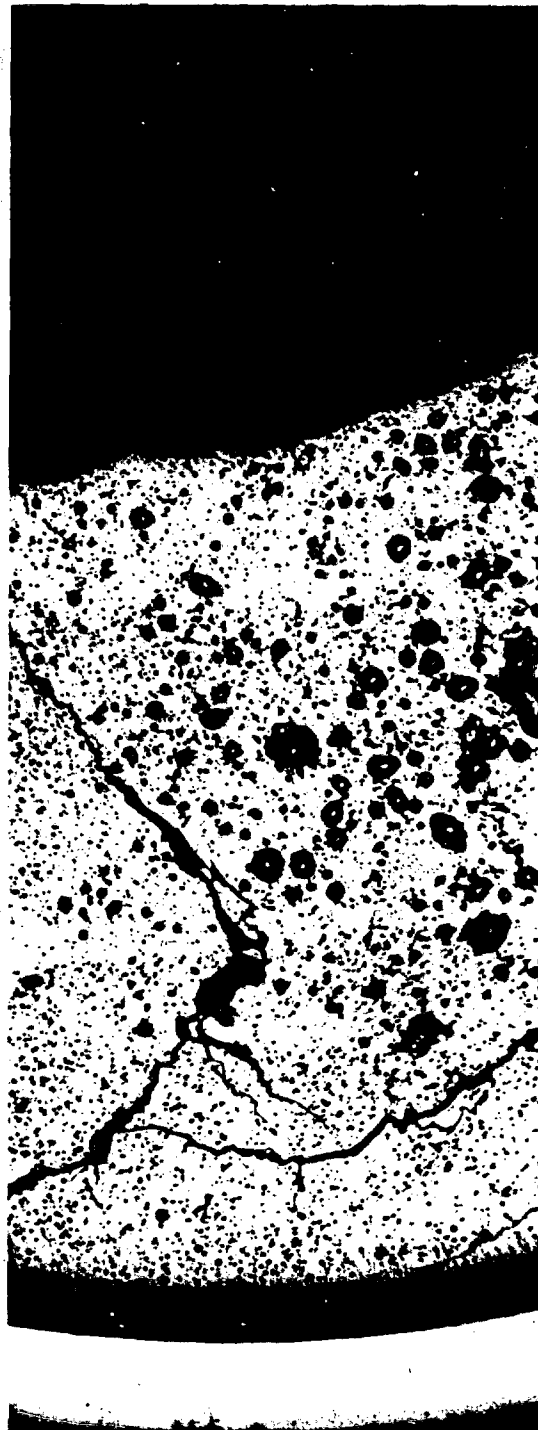
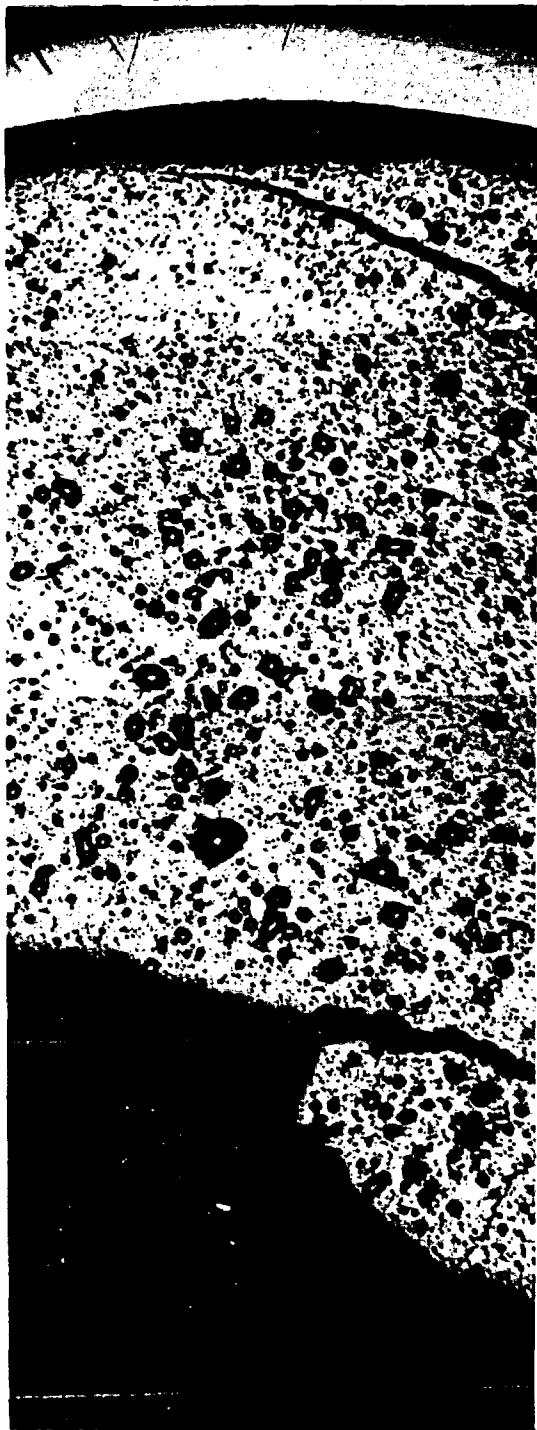


Fig. 26.

*Low temperature, fuel/cladding transverse Sec. 1B27 from OWREX-16. Cladding inner surface operated at  $\sim 610^{\circ}\text{C}$ . As-polished, 50X.*

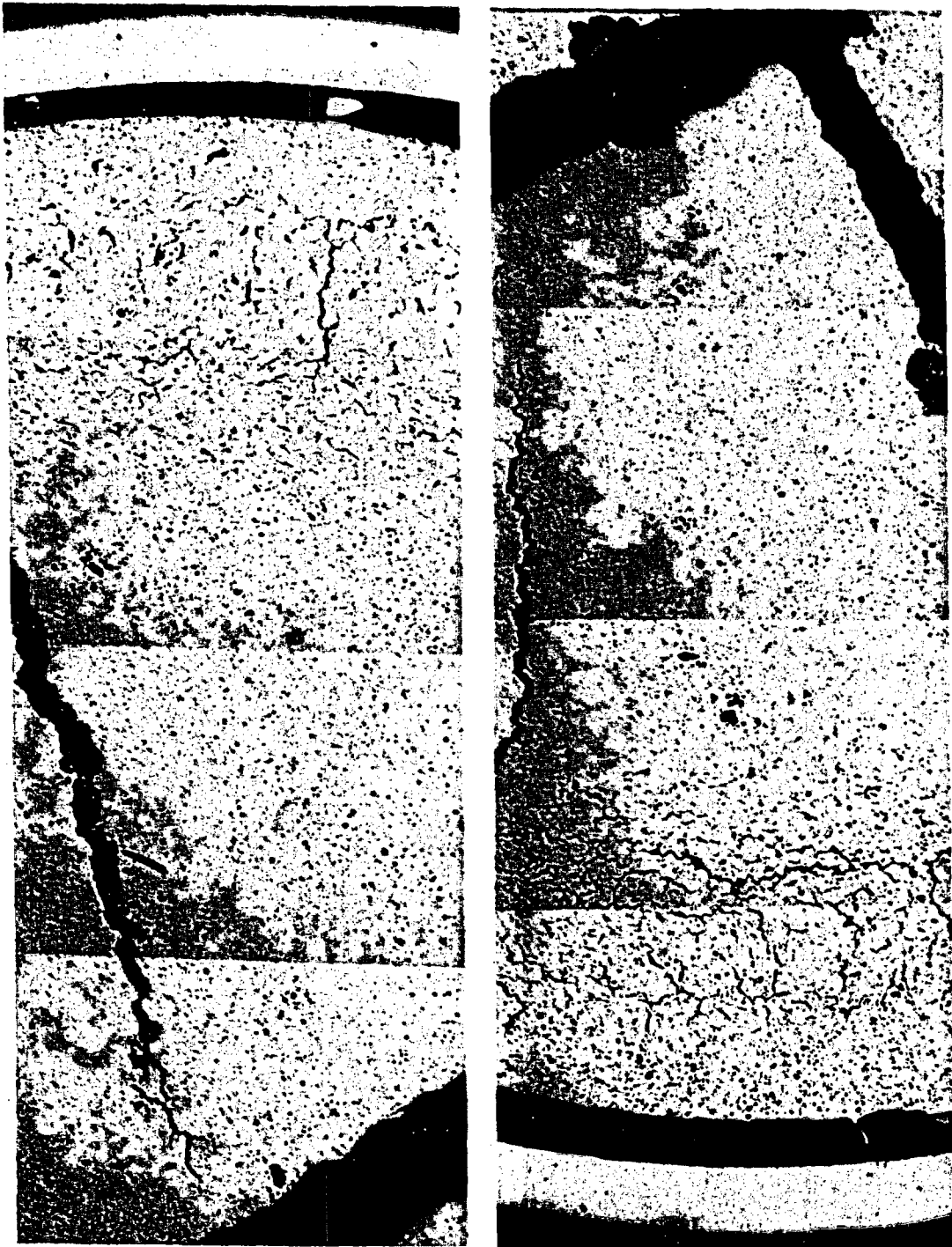
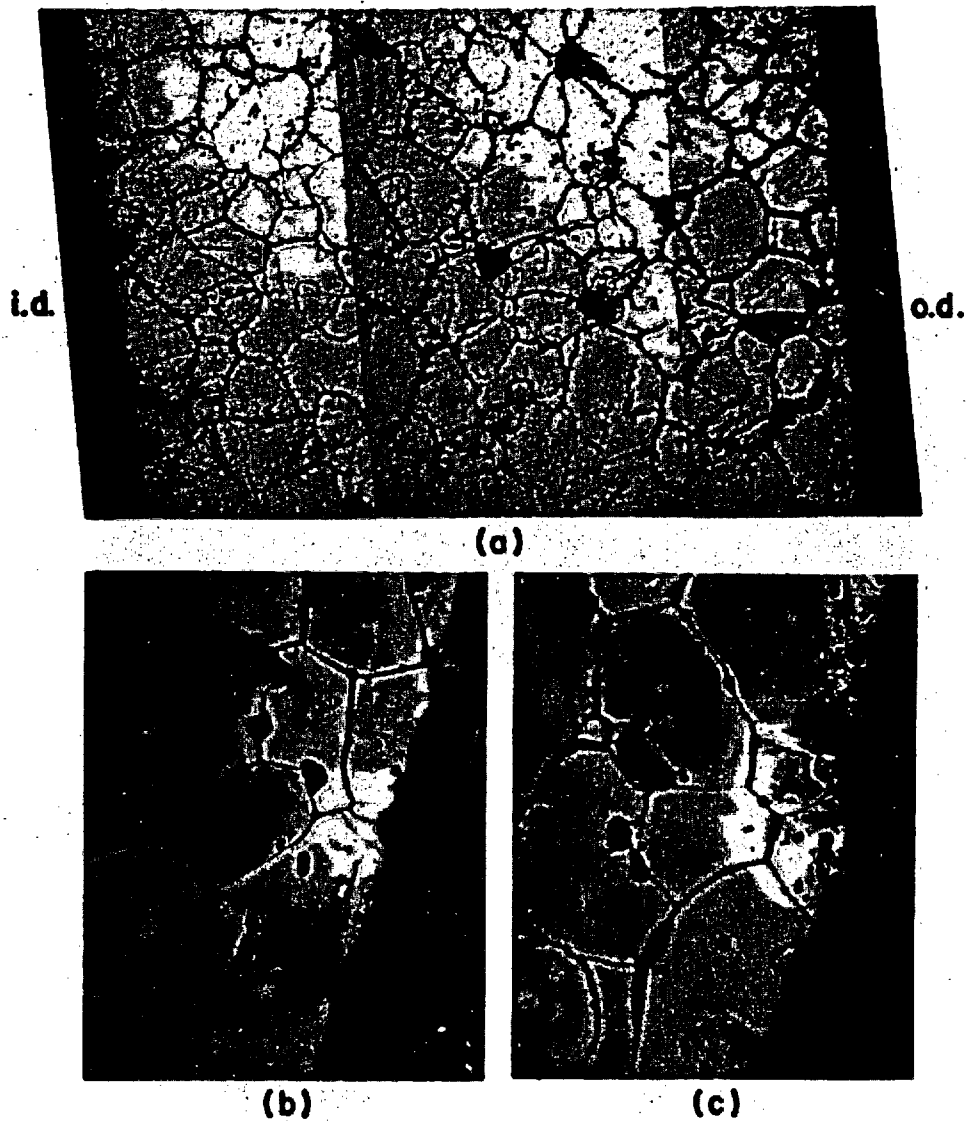
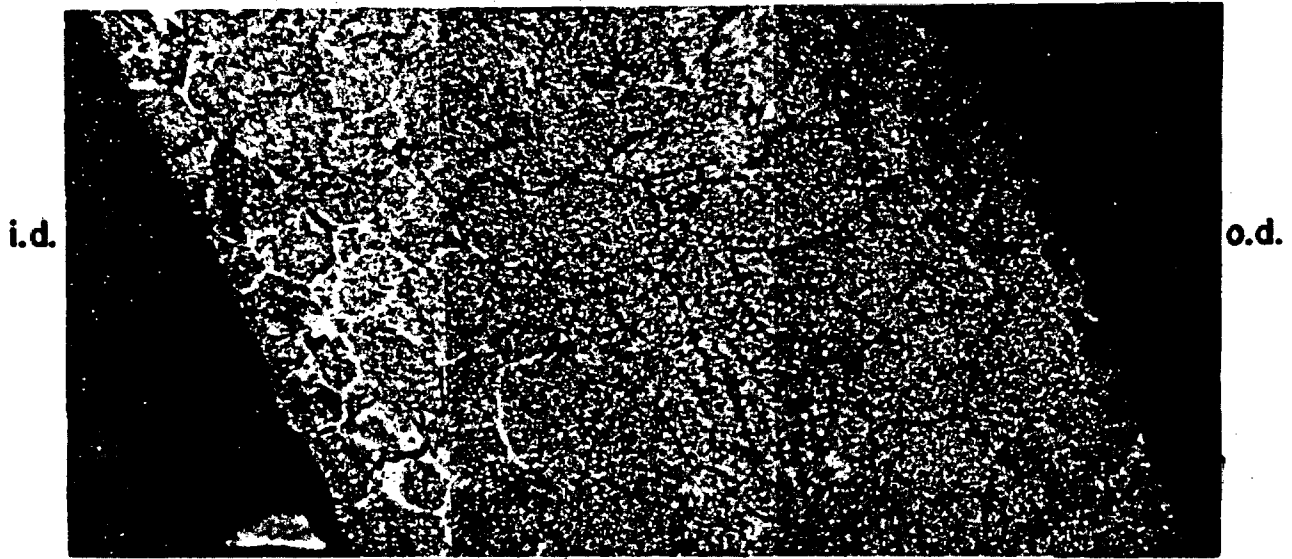


Fig. 27.

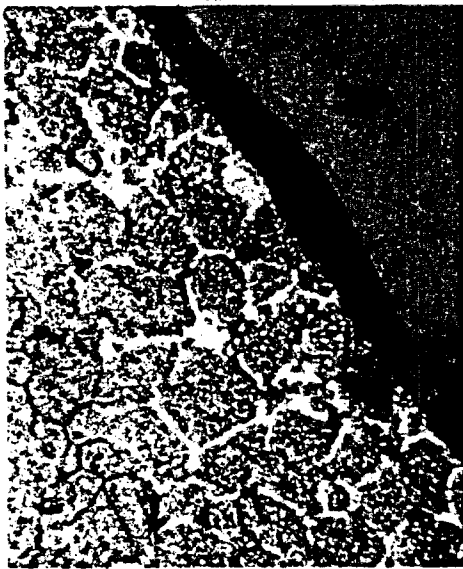
*High temperature fuel/cladding transverse Sec. 1B23 from OWREX-16. Cladding inner surface operated at  $\sim 710^{\circ}\text{C}$ . As-polished, 50X.*



**Fig. 28.**  
*Fuel/cladding transverse Sec. 1B27 from the lower temperature OWREX-16 capsule. The cladding inner surface operated at an estimated 610°C. (a) Cladding section, oxalic acid electrolytic etch, 525X, (b,c) fuel surface, lactic-acetic-nitric acid etch. 525X.*



(a)



(b)



(c)

Fig. 29.  
Type 316 stainless steel from transverse Sec. 1B23, OWREX-16. Cladding inner surface operated at an estimated 710°C. Oxalic acid electrolytic etch, 525X.

The microstructure of etched fuel in the high temperature, transverse section from OWREX-16 is shown in Fig. 30. The structure appeared unchanged from that of controls. However, the light-colored inclusions were more in evidence than would have been expected based on the results of routine metallographic inspections made on control pellets. Inclusions were visible throughout the irradiated sample, but variations in concentration with radial position, such as might be expected if the distribution of the phase were influenced by burnup or temperature gradient, could not be determined in the brief examination allotted this specimen.

Microstructures of the insulator pellets from both OWREX-16 capsules (Table VII) appear in Fig. 31. The fuel contact surface of the colder insulator pellet showed the same structure throughout: heavy intragranular precipitates to a depth of  $\sim 0.001$  in. and to a thin, intermittent, precipitate-free surface zone (Fig. 31a). The higher temperature insulator pellet was not uniform across the surface that had contacted fuel. The edges of the upper surface of the insulator pellet exhibited the heavy precipitate (Fig. 31b) observed in the OWREX-15 insulator pellet, whereas the surface at the pellet center exhibited an angular or crystalline-appearing phase beneath which some coarse, spheroidized precipitates appeared (Fig. 31c). The normal microstructure of this insulator pellet, in a region removed from the fuel contact surface, is shown in Fig. 31d.

3. Electron Beam Microprobe Examinations. Transverse fuel/cladding Sec. OA93 and insulator pellet Sec. OA98 from OWREX-15 were examined with a shielded electron beam microprobe to determine whether interdiffusion of fuel and cladding constituents had occurred. Iron, chromium, nickel, and molybdenum were detected at trace concentrations to a depth of  $100 \mu\text{m}$  beneath the fuel surface in some of the randomly selected surface regions examined, but were not observed near the center of the fuel. Silicon was detected at trace levels throughout the fuel. Composition variations were not observed in either the cladding or the insulator pellet, nor were uranium, plutonium, and carbon detected. Detection limits for stainless steel constituents in the fuel and for uranium and plutonium in the stainless steel were estimated to be in the 0.05 to 0.5 wt% range. The detection limit for carbon in stainless steel was estimated to be 1 wt% in the presence of irradiated fuel and 0.8 wt% in its absence. The fission product promethium was observed occasionally in the gap between fuel and cladding, but concentrations of other major fission products were not detected.

Fuel-cladding specimen 1B23 (Figs. 29,30) and insulator pellet 1B26 (Figs. 31a, 31b) from OWREX-16 also were examined with the shielded microprobe. Traverses of the cladding wall at randomly selected locations did not

reveal variations in iron, chromium, nickel, or molybdenum concentration, and uranium and plutonium were not detected at any cladding location. Specific attempts to correlate the white grain boundary network of Fig. 29 with changes in chromium, nickel, or molybdenum concentration were unsuccessful. Because of the poor sensitivity of the probe for carbon in the presence of irradiated fuel, scans for that element were not made.

Fuel lying within 100 to  $200 \mu\text{m}$  of the pellet surface in Sec. 1B23 was examined (Fig. 32). Significantly higher concentrations of plutonium, ruthenium, palladium, rhodium, and silicon, and significantly lower concentrations of uranium were observed in the light inclusions than in the fuel matrix. Concentrations of other major fission products were not detected. Interior regions of the fuel were not examined for possible noble metal fission product concentrations so that, although light-colored inclusions were observed here, the assumption that every light-colored inclusion contained concentrations of noble metal fission products is not warranted. Nor is the assumption warranted that all fission product containing inclusions were silicon- and plutonium-rich with respect to the matrix. A source of silicon external to the fuel was sought by examining cladding and fuel for silicon gradients. Silicon was readily observable in the cladding, but no gradient was detected. Silicon inhomogeneities were present in the fuel but, again, no gradient was detected. Therefore, it is likely that the noble metal fission product-containing inclusions observed with the microprobe were present as plutonium- and silicon-rich inclusions in the as-fabricated fuel, and that fission products migrated to these inclusions during irradiation. Noble metal-containing inclusions have been observed in carbides irradiated to 4 to 5% burnup of heavy atoms<sup>19</sup> and have been produced in lower burnup uranium carbide by a postirradiation heating technique,<sup>20</sup> so that the concentration of noble metals in inclusions in the OWREX-16 fuel is not totally unexpected.

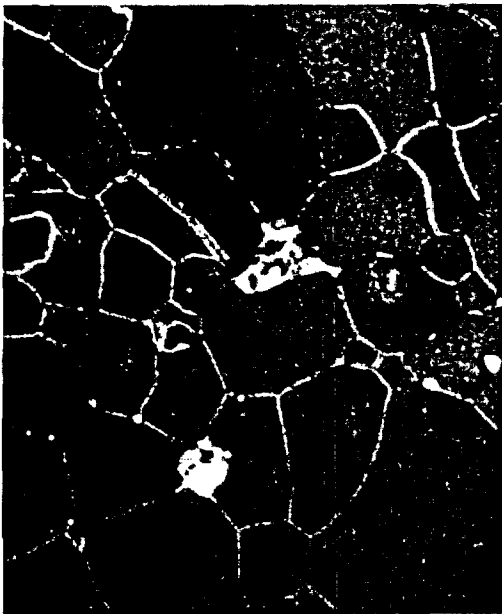
Microprobe examinations of stainless steel insulator pellet 1B28 showed slight differences in carbon content between the surface that had contacted fuel and the interior. The edges of the contact surface, corresponding to the structure in Fig. 31b, were carburized to a depth of  $\sim 100 \mu\text{m}$  beneath the surface. The central portion of the contact surface (Fig. 31c) was decarburized to approximately the same depth. With the exception of carbon, no evidence was found to suggest that fuel-clad interaction had occurred. Possible contributors to the difference in behavior along the insulator pellet surface include the radial temperature gradient through the fuel and the varying proximity of fuel and insulator pellet because of the concavity of the fuel pellet end surfaces.



(a)



(b)



(c)



(d)

Fig. 30.

*Fuel transverse Sec. 1B23, OWREX-16, after irradiation to surface burnup of ~13 at.%. Lactic-acetic-mitric acid etch, 525X. (a) Fuel surface, (b, c) outer 0.020 in. of fuel, (d) fuel center.*

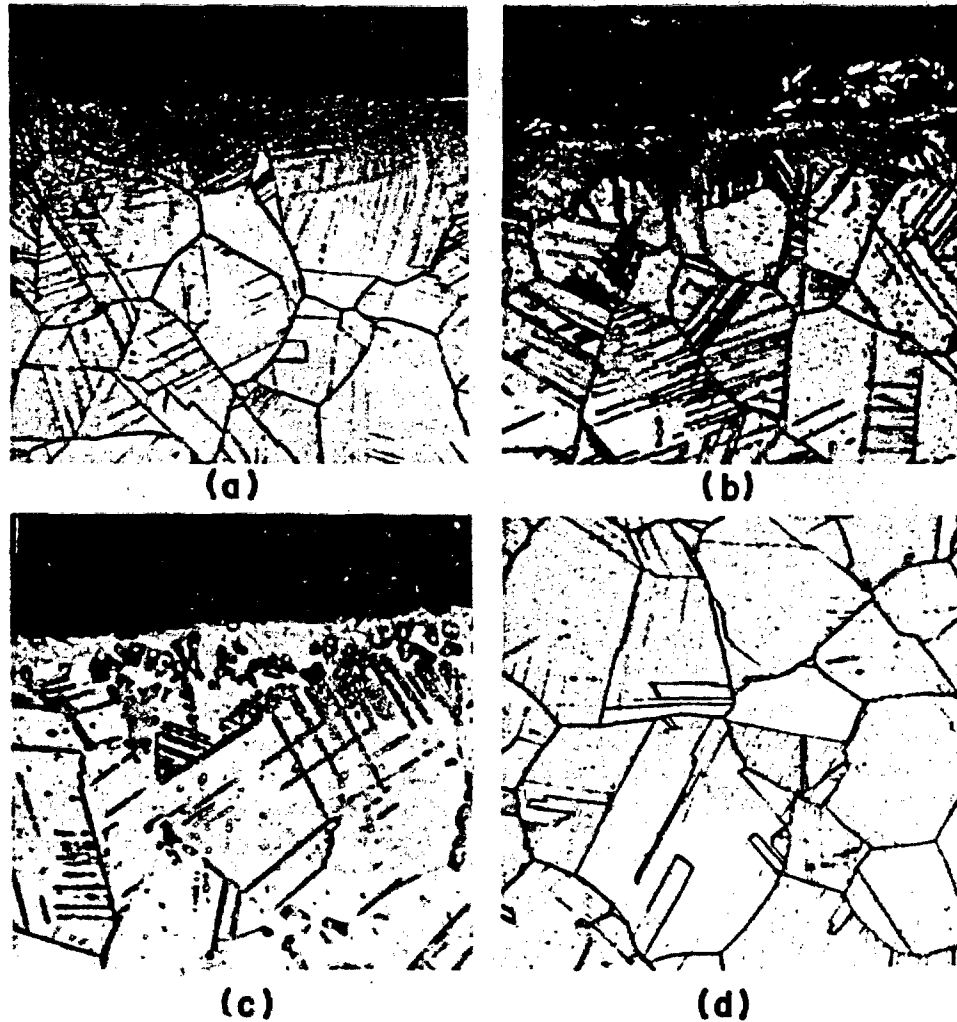


**Fig. 31.**  
*Type 316 stainless steel insulator pellets 1B26 and 1B28, OWREX-16. Surfaces in contact with fuel operated at estimated temperatures of 570 to 600°C. Oxalic acid electrolytic etch, 525X. (a) Lower temperature insulator pellet surface, (b) higher temperature insulator pellet surface at corner, (c) higher temperature insulator pellet surface at center, and (d) higher temperature insulator pellet interior.*



Fig. 32.

*OWREX-16 fuel, transverse Sec. 1B23 adjacent to fuel pellet surface, as-polished, 525X. Microprobe examination of darkened area revealed small regions enriched in noble metal fission products. Light blob at edge of darkened region was caused by release of entrapped sodium from the fuel.*

#### IV. DISCUSSION

Although postirradiation microprobe examinations of the capsule material generally were inconclusive, tentative explanations of the major microstructural changes can be made based on the similarity between postirradiation structures and the structures observed after out-of-pile compatibility tests. Qualitative identification of alloy constituents was possible after out-of-pile tests, partly because of the absence of radioactive decay and associated photons.

Litton<sup>7,21</sup> studied the interaction of the solid solution monocarbide and the monocarbide containing higher carbides, with sodium and Type 316 stainless steel in the 450 to 750°C range. When carbon was transported from fuel to cladding at 650°C or less, the stainless steel structures shown in Fig. 33 resulted. Microprobe studies confirmed the presence of carbon in higher concentration than in the unaffected matrix, in the dark, broad grain boundaries adjacent to the cladding surface in Fig. 33a, to a 150- $\mu$ m depth beneath the surface in Fig. 33b, to a 50- $\mu$ m depth

beneath the surface in Fig. 33c, and throughout the structure in Fig. 33d. The similarity between these structures and the structures observed after the thermal neutron irradiations (Figs. 23, 24, and 28) suggests that the dark, inter- and intragranular precipitates observed after irradiation also contain carbon.

After heating times >1000 h at 750°C out-of-pile, Type 316 stainless steel that had not been carburized by the fuel developed the structure shown in Fig. 34a.<sup>21</sup> The dark, overetched regions appearing at grain boundaries and triple points were identified as the iron-chromium Sigma phase, and the small intragranular precipitates were  $M_{23}C_6$ -type carbides. At higher magnification these carbides gave the structure a mottled appearance. Carbide precipitates were not visible in the grain boundaries, which appeared as a white network after etching with oxalic acid. When cladding carburization took place out-of-pile at 750°C, chromium apparently was removed from the stainless steel matrix as a complex carbide, reducing the tendency for Sigma phase formation. Figures 34b and 34c show the structure formed when hyperstoichiometric carbide fuel caused carburization of the inside (lower) surface of two Type 316 stainless steel capsules. In each carburized zone, inter- and intragranular carbide precipitates have formed and only small amounts of the Sigma phase are visible. Toward the outside (upper) surface of the cladding the amount of Sigma phase increased, the carbide precipitates were confined to the grains, and a white grain boundary network appeared.

The microstructural similarities between irradiated and unirradiated Type 316 stainless steel sodium-bonded to mixed carbide fuel suggest that the major features of the cladding after irradiation can be explained by a combination of localized carburization and normal, high temperature aging. Where carbon transfer did not occur during several thousand hours at elevated temperature in-pile, the Sigma phase formed, depleting grain boundaries and the adjacent regions of chromium, which prevented the formation of chromium-containing complex carbides and produced the white network visible in the inner third of the wall in Figs. 29a and 29b. The lack of Sigma phase in the remaining two-thirds of the wall in Fig. 29a may be attributed to two circumstances: (1) carburization of the cladding by the secondary bonding sodium (evident in the OWREX-16 lower capsule, Fig. 28a), and (2) reduction of the tendency for Sigma phase formation in the cooler outer portions of the cladding. At lower temperature or after shorter time above 700°C, and in the absence of significant carbon transport from the fuel, the clad inner surfaces appeared unchanged, as illustrated by the OWREX-16 lower capsule (Fig. 28a) and the OWREX-14 upper capsule (Fig. 23).

All the insulator pellets (Figs. 23, 24, and 31) and a few regions of the clad inner surface (Fig. 29c) exhibited

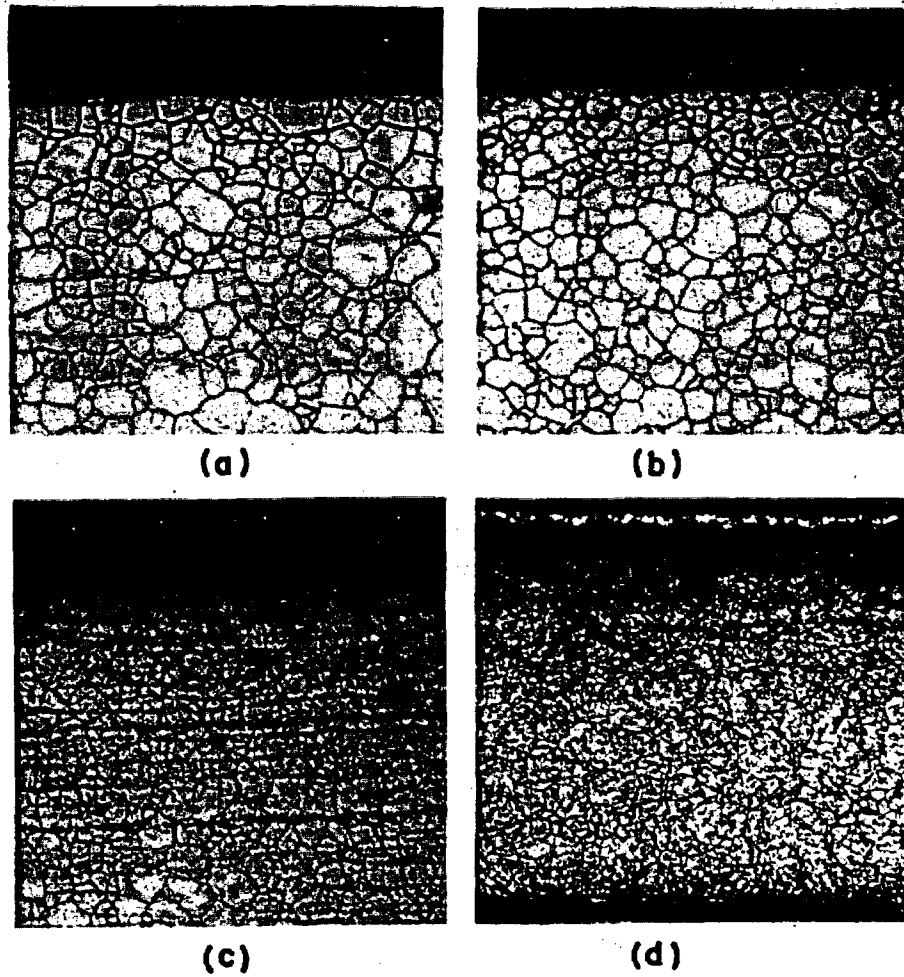
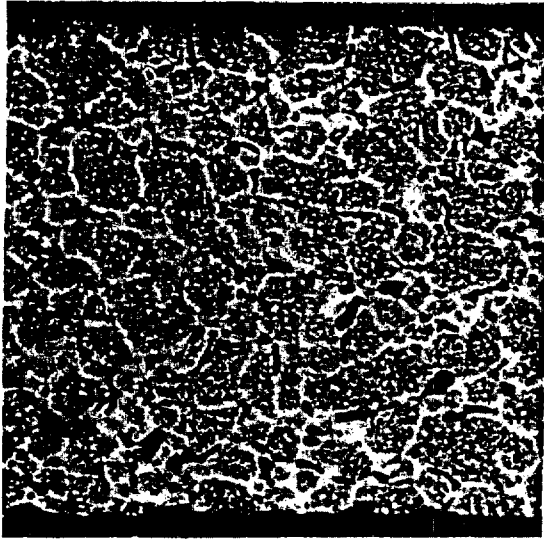
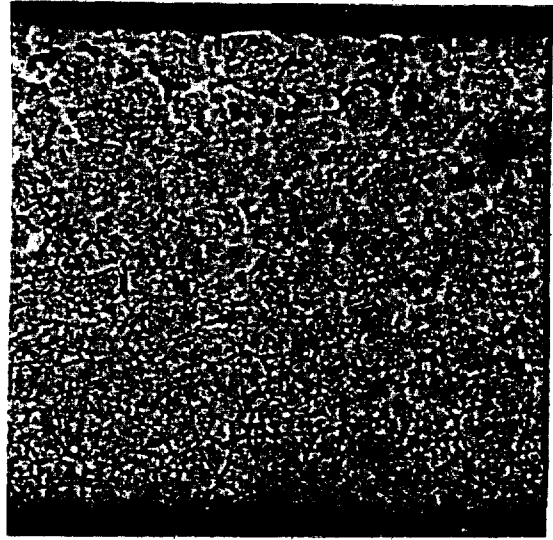


**Fig. 33.**

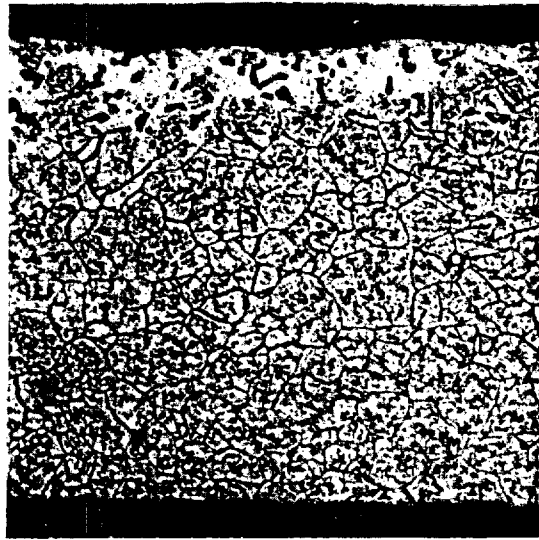
*Carburization of Type 316 stainless steel that was sodium-bonded to stoichiometric and hyperstoichiometric, solid solution carbides. Oxalic acid electrolytic etch, 300X. (a) stoichiometric fuel, 1000 h at 550°C, (b) hyperstoichiometric fuel, 1000 h at 650°C, (c) hyperstoichiometric fuel, 1000 h at 750°C, and (d) hyperstoichiometric fuel, 4000 h at 700°C.*



(a)



(b)



(c)

*Fig. 34.*

*Aging and carburization of Type 316 stainless steel after 4000 h contact with sodium-bonded stoichiometric and hyperstoichiometric carbides. Oxalic acid electrolytic etch, 300X. (a) 750°C, uncarbided.*

a thin, white surface zone that was free of carbide precipitates. Usually an adjacent zone of heavy carbide precipitation was visible. Similar surface changes were observed after out-of-pile compatibility tests and flowing sodium tests using solid solution carbides.<sup>22,23</sup> In general, these layers were depleted in carbon, chromium, and molybdenum with respect to the matrix, and were enriched in nickel and iron, while the underlying zone of heavy carbide precipitation was iron- and nickel-poor.

A cladding surface layer containing nickel and plutonium also has been reported after 8000 h contact out-of-pile between Type 316 stainless steel, single phase (U,Pu)C, and sodium at 750°C.<sup>24</sup> The Sigma phase was present in the cladding, and an explanation for the surface layer was postulated, involving the depletion of chromium from the cladding matrix (to form the Sigma phase) and the reaction of the resulting nickel-rich cladding with plutonium from the fuel.

Conveniently for this argument, changes in the surface composition of a Type 316 stainless steel capsule were noted following irradiation of sodium-bonded (U,Pu)C in a fast flux.<sup>25</sup> During operation to a fuel burnup of ~4.4 at.% at cladding temperatures of 515 to 680°C, the stainless steel inner surfaces experienced movement of iron and nickel, or nickel alone, from a subsurface zone a few microns thick to the surface. Sometimes nickel and iron depletion in the zone was accompanied by chromium enrichment. Plutonium and uranium were not detected in the cladding of the fast neutron irradiation experiment.

In the absence of positive microprobe results, the nature of the white layers at the OWREX cladding and insulator pellet surfaces cannot be stated. However, the results of the other investigations cited above suggest that these narrow, white surface layers are associated with changes in alloy composition. Although the mechanism of layer formation is unknown, the layers are thin and of no apparent consequence.

The remaining cladding microstructural feature observed after OWREX irradiations was the loss of grains from the inside surface of the cladding. The effect was confined to the OWREX-14 and -15 capsules, which were sectioned and stored for different periods before examination and then were examined together. Additionally, the grain loss was not confined to the fuel-containing portions of the capsules but occurred in the gas spaces as well. Because the grain loss was random in two experiments and was not observed at all in the third, it is assumed to have resulted from some peculiarity in the storage or processing of these metallographic specimens.

## V. CONCLUSIONS

The limited number of experiments conducted, together with the difference from the operating conditions expected in a fast reactor, make broad conclusions concerning the stability of sodium-bonded mixed carbides after high burnup in a fast flux risky. However, some limited observations are possible which are of value for the fast flux irradiation experiments under way. Chemical compatibility among the fuel, sodium, and cladding of these experiments was satisfactory, and no attack of fuel and only minor cladding carburization were observed. The origin of the phase containing concentrations of noble metal fission products, plutonium, and silicon above those in the fuel matrix is unknown, but the phase appeared to be benign in these tests. There is no reason to expect different behavior in fast flux irradiations. Of more concern is the observed fragmentation of the fuel under thermal stress and the possibility that fragments may become wedged in the sodium-bond annulus and cause fuel-clad mechanical interaction. Proper evaluation of the seriousness of fuel fragmentation can be made only in full-length fuel columns operating at power densities, radial temperature gradients, and fast fluences of interest. Another phenomenon whose importance can be judged only after fast flux irradiations is thermal aging of Type 316 stainless steel. Aging results in precipitation of the brittle Sigma phase and would be expected to have deleterious effects on mechanical properties of the cladding. Mechanical property degradation by this mechanism may be trivial in comparison with that produced by fast neutrons, but aging would appear to be a complication that could be avoided by substitution of another austenitic stainless steel for Type 316 stainless steel.

## ACKNOWLEDGMENTS

I wish to thank the members of the Reactor, Experimental Physics, Chemistry-Metallurgy, and Explosives Systems Divisions of LASL for their help in conducting these experiments. Special thanks to R. L. Cubitt and D. C. Kirkpatrick for assistance in refurbishing and operating the irradiation facilities, and to H. E. Strohm, A. E. Vandergust, and L. L. Marriott for preparing and operating the experiments. I am grateful to J. A. Yarnell, H. T. Williams, and the OWR staff for assistance in operating and monitoring the experiments; to J. A. Leary for fuel fabrication; to D. N. Dunning, J. O. Barner, and J. W. Woolsey for assistance in fuel capsule preparation; to J. F.

Torbert, J. R. Phillips, and J. B. Finley for nondestructive examination of capsules and assemblies; to G. R. Waterbury, J. W. Schulte, and K. A. Johnson for assistance in planning and guiding postirradiation examinations; to W. F. Zelezney, E. A. Hakkila, and J. M. Hansel for shielded microprobe examinations; to J. H. Bender for metallographic examinations; to F. Fitzgibbon and the hot cell staff for disassembly and inspection of irradiated experiments; to R. E. Alcouffe for burnup calculations; and to F. B. Litton for data on the aging of carburized stainless steels. I also thank D. B. Hall, R. E. Peterson, and R. D. Baker for their support and encouragement during the course of the work.

## REFERENCES

1. Combustion Engineering, Inc., "1000 MWe Liquid Metal Fast Breeder Reactor Follow-On Study, Summary Description of the C-E Reference Design," paper presented at Intern. Conf. on Sodium Technology and Large Fast Reactor Design, Argonne National Laboratory, Argonne, Illinois, November 7-9, 1968.
2. C. E. Shufelt, Ed., "Westinghouse 1000 MWe Fast Breeder Reactor, Summary Description of Conceptual Plant Design," paper presented at Intern. Conf. on Sodium Technology and Large Fast Reactor Design, Argonne National Laboratory, Argonne, Illinois, November 7-9, 1968.
3. Liquid Metal Fast Breeder Program Office, "Liquid Metal Fast Breeder Reactor Program Plan," USAEC Research and Development report No. WASH 1107, Vol. 7, p. 154, (August 1968).
4. F. B. Litton, "The Properties and Irradiation Behavior of Carbide Fuels: A Literature Survey," Los Alamos Scientific Laboratory report LA-3799 (March 1968).
5. R. Powers and A. Strasser, "Compatibility of Several Cladding Materials with Uranium-Plutonium-Carbides in Sodium," United Nuclear Corporation report UNC 5229 (November 1968).
6. M. W. Shupe, A. E. Ogard, and J. A. Leary, "Synthesis and Fabrication of Pure, Single-Phase, Uranium-Plutonium Monocarbide Pellets," Los Alamos Scientific Laboratory report LA-4283 (March 1970).
7. F. B. Litton and T. C. Wallace, Jr., "The Stability of Sodium-Bonded Actinide Carbides in Type 316 Stainless Steel Containers," paper presented at the 100th Annual Meeting of the AIME, New York, March 1-5, 1971.
8. H. T. Williams, O. W. Stopinski, J. L. Yarnell, A. R. Lyle, C. L. Warner, and H. L. Maine, "1969 Status Report on the Omega West Reactor, with Revised Safety Analysis," Los Alamos Scientific Laboratory report LA-4192 (July 1969).
9. R. L. Cubitt, G. L. Ragan, D. C. Kirkpatrick, "Thermal Irradiation of Liquid Plutonium-Alloy Fuels," Los Alamos Scientific Laboratory report LA-3832 (June 1968).
10. C. B. Becherer and A. R. Vandergust, "Design Report, OWREX Control and Monitoring System, Environmental Cells 1 & 2," Los Alamos Scientific Laboratory, internal document, March 1970.
11. D. N. Dunning, "Loading of Sodium-Bonded Fuel Capsules," Los Alamos Scientific Laboratory report LA-4393 (March 1970).
12. D. H. Holm, W. M. Sanders, J. L. Parker, H. D. Cowan, "Examination of Fast Reactor Fuel Elements with a Ge(Li) Anticoincidence Gamma-Ray Spectrometer," Proc. 16th ANS Conf. on Remote Systems Technology, Idaho Falls, Idaho, March 11-12, 1969, pp. 228-242.
13. K. D. Lathrop, "DTF-IV, A Fortran-IV Program for Solving the Multigroup Transport Equation with Anisotropic Scattering," Los Alamos Scientific Laboratory report LA-3373 (July 1965).
14. G. E. Hansen and W. H. Roach, "Six and Sixteen Group Cross Sections for Fast and Intermediate Critical Assemblies," Los Alamos Scientific Laboratory report LAMS-2543 (December 1961).
15. W. H. McAdams, *Heat Transmission* (McGraw-Hill Publishing Company, New York, 3rd ed.) 1954, pp. 12-19.
16. R. E. Alcouffe, Los Alamos Scientific Laboratory, personal communication, May 1971.
17. J. R. Phillips, Los Alamos Scientific Laboratory, personal communication.
18. C. E. Frantz, P. A. Mason, and C. D. Montgomery, "Inert Atmosphere Hot Cells for the Examination of Irradiated U-Pu Fuel Elements," Proc. 19th Conf. on Remote Systems Technology, American Nuclear Society, Miami Beach, Florida, October 1971, p. 32.
19. J. I. Bramman, R. M. Sharpe, and R. Dixon, "Fission-Product Inclusion in Irradiated Uranium-Plutonium Carbide," *J. Nucl. Mater.* 38, 226-229 (1971).
20. N. Oi, "Behavior of Fission Product Ruthenium in Uranium Carbide," *J. Nucl. Mater.* 34, 227-229 (1970).
21. F. B. Litton, H. A. O'Brien, and L. A. Geoffrion, "Carbide Fuel Compatibility Studies" in Los Alamos Scientific Laboratory "Quarterly Status Report on the Advanced Plutonium Fuels Program, October 1 to December 31, 1969," LA-4376-MS (February 1970), pp. 29-35.
22. F. B. Litton, Los Alamos Scientific Laboratory, internal document, October 1968.
23. J. C. Clifford, Los Alamos Scientific Laboratory, internal document, November 1968.

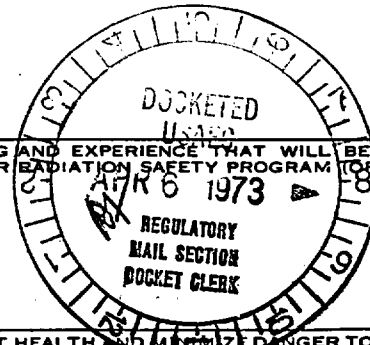
24. F. B. Litton, H. A. O'Brien, and L. A. Geoffrion, "Carbide Fuel Compatibility Studies," in Los Alamos Scientific Laboratory "Quarterly Status Report on the Advanced Plutonium Fuels Program, April 1 - June 30, 1970," and Fourth Annual Report, FY 1970," LA-4494-MS (August 1970), p. 57.
25. J. O. Barner, "Behavior of Sodium-Bonded (U,Pu)C Fuel Elements after Moderate Burnup," Amer. Nucl. Soc. proceedings of Fast Reactor Fuel Element Technology, New Orleans, Louisiana, May 1971.

APPLICATION FOR SOURCE MATERIAL LICENSE

REGULATORY FILE CY

Pursuant to the regulations in Title 10, Code of Federal Regulations, Chapter 1, Part 40, application is hereby made for a license to receive, possess, use, transfer, deliver or import into the United States, source material for the activity or activities described.

1. (Check one) <input type="checkbox"/> (a) New license <input checked="" type="checkbox"/> (b) Amendment to License No. <u>SUB-1150</u> <input type="checkbox"/> (c) Renewal of License No. _____ <input type="checkbox"/> (d) Previous License No. _____		2. NAME OF APPLICANT <u>Department of the Army, US Army Electronics Command</u>	
4. STATE THE ADDRESS(ES) AT WHICH SOURCE MATERIAL WILL BE POSSESSED OR USED  <u>No Change</u>		3. PRINCIPAL BUSINESS ADDRESS <u>ATTN: AMSEL-SF</u> <u>Fort Monmouth, New Jersey 07703</u>	
5. BUSINESS OR OCCUPATION <u>No Change</u>	6. (a) IF APPLICANT IS AN INDIVIDUAL, STATE CITIZENSHIP <u>N/A</u>	(b) AGE <u>N/A</u>	
7. DESCRIBE PURPOSE FOR WHICH SOURCE MATERIAL WILL BE USED <u>ADD:</u> <u>SOURCE C. Source material will be used to check operation of radiation detection equipment, specifically the AN/PDR-56 radiac instrument.</u>			
8. STATE THE TYPE OR TYPES, CHEMICAL FORM OR FORMS, AND QUANTITIES OF SOURCE MATERIAL YOU PROPOSE TO RECEIVE, POSSESS, USE, OR TRANSFER UNDER THE LICENSE			
(a) TYPE	(b) CHEMICAL FORM	(c) PHYSICAL FORM (Including % U or Th.)	(d) MAXIMUM AMOUNT AT ANY ONE TIME (in pounds)
NATURAL URANIUM			
URANIUM DEPLETED IN THE U-235 ISOTOPE			
<sup>232</sup> THORIUM (ISOTOPE)	<u>ADD:</u> <u>Source C. Metal Sheet</u>	<u>Metal Sheet, 99.99%</u> <u>Th-232</u>	<u>110</u>
(e) MAXIMUM TOTAL QUANTITY OF SOURCE MATERIAL YOU WILL HAVE ON HAND AT ANY TIME (in pounds) <u>112.2</u>			
9. DESCRIBE THE CHEMICAL, PHYSICAL, METALLURGICAL, OR NUCLEAR PROCESS OR PROCESSES IN WHICH THE SOURCE MATERIAL WILL BE USED, INDICATING THE MAXIMUM AMOUNT OF SOURCE MATERIAL INVOLVED IN EACH PROCESS AT ANY ONE TIME, AND PROVIDING A THOROUGH EVALUATION OF THE POTENTIAL RADIATION HAZARDS ASSOCIATED WITH EACH STEP OF THOSE PROCESSES.  <u>See Supplement One</u>			
10. DESCRIBE THE MINIMUM TECHNICAL QUALIFICATIONS INCLUDING TRAINING AND EXPERIENCE THAT WILL BE REQUIRED OF APPLICANT'S SUPERVISORY PERSONNEL INCLUDING PERSON RESPONSIBLE FOR RADIATION SAFETY PROGRAM (IF APPLICANT IS AN INDIVIDUAL).  <u>No Change</u>			
11. DESCRIBE THE EQUIPMENT AND FACILITIES WHICH WILL BE USED TO PROTECT HEALTH AND MINIMIZE DANGER TO LIFE OR PROPERTY AND RELATE THE USE OF THE EQUIPMENT AND FACILITIES TO THE OPERATIONS LISTED IN ITEM 9. INCLUDE: (a) RADIATION DETECTION AND RELATED INSTRUMENTS (including film badges, dosimeters, counters, air sampling, and other survey equipment as appropriate. The description of radiation detection instruments should include the instrument characteristics such as type of radiation detected, window thickness, and the range(s) of each instrument). <u>ADD:</u> <u>Source C. Radiac instrument AN/PDR-56 will be used to detect presence of the source material. This instrument is a scintillation type alpha particle radiation intensity measuring device.</u>			
(b) METHOD, FREQUENCY, AND STANDARDS USED IN CALIBRATING INSTRUMENTS LISTED IN (a) ABOVE, INCLUDING AIR SAMPLING EQUIPMENT (for film badges, specify method of calibrating and processing, or name supplier). <u>ADD: Radiac instruments AN/PDR-56 are calibrated at the factory and further calibration is not required unless critical parts are changed. The procedure when required is as described in the manual, a copy of which is attached as Supplement 3A.</u>			



Encl 11

11(c). VENTILATION EQUIPMENT WHICH WILL BE USED IN OPERATIONS WHICH PRODUCE DUST, FUMES, MISTS, OR GASES, INCLUDING PLAN VIEW SHOWING TYPE AND LOCATION OF HOOD AND FILTERS, MINIMUM VELOCITIES MAINTAINED AT HOOD OPENINGS AND PROCEDURES FOR TESTING SUCH EQUIPMENT.

N/A

12. DESCRIBE PROPOSED PROCEDURES TO PROTECT HEALTH AND MINIMIZE DANGER TO LIFE AND PROPERTY AND RELATE THESE PROCEDURES TO THE OPERATIONS LISTED IN ITEM 9: INCLUDE: (a) SAFETY FEATURES AND PROCEDURES TO AVOID NONNUCLEAR ACCIDENTS, SUCH AS FIRE, EXPLOSION, ETC., IN SOURCE MATERIAL STORAGE AND PROCESSING AREAS.

ADD: Source C. Caution notices regarding the Thorium check source are located at various places in the technical manual for the AN/PDR-56. Extracts are attached as Supplement 4A.

(b) EMERGENCY PROCEDURES IN THE EVENT OF ACCIDENTS WHICH MIGHT INVOLVE SOURCE MATERIAL.

See Supplement Five.

(c) DETAILED DESCRIPTION OF RADIATION SURVEY PROGRAM AND PROCEDURES.

See Supplement Six.

13. WASTE PRODUCTS: If none will be generated, state "None" opposite (a), below. If waste products will be generated, check here  and explain on a supplemental sheet:

- (a) Quantity and type of radioactive waste that will be generated.
- (b) Detailed procedures for waste disposal.

14. IF PRODUCTS FOR DISTRIBUTION TO THE GENERAL PUBLIC UNDER AN EXEMPTION CONTAINED IN 10 CFR 40 ARE TO BE MANUFACTURED, USE A SUPPLEMENTAL SHEET TO FURNISH A DETAILED DESCRIPTION OF THE PRODUCT, INCLUDING:

- (a) PERCENT SOURCE MATERIAL IN THE PRODUCT AND ITS LOCATION IN THE PRODUCT.
- (b) PHYSICAL DESCRIPTION OF THE PRODUCT INCLUDING CHARACTERISTICS, IF ANY, THAT WILL PREVENT INHALATION OR INGESTION OF SOURCE MATERIAL THAT MIGHT BE SEPARATED FROM THE PRODUCT.
- (c) BETA AND BETA PLUS GAMMA RADIATION LEVELS (Specify instrument used, date of calibration and calibration technique used) AT THE SURFACE OF THE PRODUCT AND AT 12 INCHES.
- (d) METHOD OF ASSURING THAT SOURCE MATERIAL CANNOT BE DISASSOCIATED FROM THE MANUFACTURED PRODUCT.

### CERTIFICATE

(This item must be completed by applicant)

15. The applicant, and any official executing this certificate on behalf of the applicant named in Item 2, certify that this application is prepared in conformity with Title 10, Code of Federal Regulations, Part 40, and that all information contained herein, including any supplements attached hereto, is true and correct to the best of our knowledge and belief.

Department of the Army  
US Army Electronics Command

(Applicant named in Item 2)

Dated 29 January 1973

BY: Bernard M. Savaiko  
(Print or type name under signature)

BERNARD M. SAVAIKO  
USAECOM Safety Director

(Title of certifying official authorized to act on behalf of the applicant)

WARNING: 18 U.S.C. Section 1001; Act of June 25, 1948; 62 Stat. 749; makes it a criminal offense to make a willfully false statement or representation to any department or agency of the United States as to any matter within its jurisdiction.

## Supplement One

ADD:

Source C. This item is TRACERLAB Part No. B238020. Each item contains less than 2.73 microcuries of Thorium-232 in the form of a metal sheet 2-1/4 by 2-3/4 by 0.02 inches weighing 0.055 pounds. This metal sheet is bonded to the underside of the case of the AN/PDR-56 radiacmeter. These items are used individually as a check source to check the operation of the AN/PDR-56 radiac instrument. Potential hazards associated with these items are the ingestion of the source material by personnel or the absorption of the source material into the blood stream of personnel through cuts in the skin.

Supplement 3A

The attached sheets are copies of pages of the technical manual for the AN/PDR-56.

TABLE 6-1 ROUTINE MAINTENANCE CHECK CHART

What to Check	When to Check	How to Check	Precautions
Battery Condition	Monthly	Turn function switch to BATT. Meter reading should be greater than the minimum as indicated by vertical mark at the extreme left of the BATT. section.	Return range switch to OFF after test.
Exterior front panel Radiac set	Monthly	Wipe with clean dry cloth, removing all dirt and dust.	Do not touch Thorium check source.
Radiacmeter front panel screws	Monthly	Screws should seat firmly.	Do not tighten excessively. A loose screw will permit leakage of the case.
Probe Screws	Monthly	Screws should seat firmly.	Do not tighten excessively. A loose screw will permit leakage of the case.
Range Switch Knob	Monthly	If knob is loose tighten with Allen wrench.	Do not tighten excessively.
Handle, captive Screw	Monthly	Adjust to finger tightness	None
Radiacmeter Circuit	Monthly	See para. 3-4	Do not touch Thorium check source.
Headset	Monthly	Remove dirt, check tightness of screws and connections.	None

## 6-3. PERFORMANCE STANDARDS

## WARNING

CALIBRATION OF THE RADIAC SET, AN/PDR-56A MAY BE UNDERTAKEN ONLY BY QUALIFIED RADIAC REPAIR PERSONNEL AT AN AUTHORIZED FACILITY.

a. General - Radiac Set AN/PDR-56A was calibrated when manufactured and complete calibration is not usually required unless certain critical components are replaced. Calibration should not be attempted until the Radiac Set has been stabilized at room temperatures. In addition,

it should be allowed to run for approximately 20 minutes before any adjustment. If the PM tube has been changed or the probe opened, no adjustment should be made for at least 2 hours and preferably the probe should be dark acclimated overnight.

b. Calibration - Recalibration must always be performed when the following critical components are changed

1. Printed Circuit boards (A1, A2, A4)
2. PM Tube (V1)
3. Light pipe and screen (MP5)
4. Transformer (T1)

1. Partial Calibration

Partial calibration only will be necessary if the Printed Circuit Boards or the Light Pipe and Screen are changed.

2. Complete Calibration

Complete calibration is necessary if the transformer or photomultiplier tube is changed.

**CAUTION**

The photomultiplier must never be exposed to light when the high voltage is on the tube. Exposure to light will cause the photomultiplier tube to saturate with consequent damage and shortened tube life.

The following equipment is necessary for complete calibration:

**NOTE**

These calibration sources are not part of the Radiac Set AN/PDR-56A.

1. Four, thin, uniformly distributed Plutonium 239 sources. These must be large enough to provide complete coverage of the sensitive area. Stainless steel plates 5.5 ins. by 3.25 ins. and 0.05 ins. thick covered with Pu 239 with concentrations of 6,000  $\mu\text{gms}/\text{m}^2$ , 600  $\mu\text{gms}/\text{m}^2$ , 60  $\mu\text{gms}/\text{m}^2$  and 6  $\mu\text{gms}/\text{m}^2$  have

been found satisfactory. For explanatory purposes, sources of these values will be assumed in the following procedures.

2. An electrostatic voltmeter 0-1500 volts dc.

3. A VTVM with a range between 0.5V dc and 1.5V dc that can be read clearly.

4. A calibration jig which will ensure that there is approximately 1/32" clearance between the probe face and the source to provide reproducible positioning.

c. Partial Calibration - This calibration would be performed in the following manner:

1. Open the radiacmeter case.
2. Monitor the High Voltage with the Electrostatic Voltmeter between pin 1 Printed Circuit Board A3 and ground.
3. Monitor the discriminator bias with the VTVM between the base and emitter of transistor Q2. (Base positive with respect to emitter.)
4. Place the main probe and the 600  $\mu\text{gms}/\text{m}^2$  source in the calibration jig, as shown in figure 6-1.
5. Check the mechanical zero of the meter.
6. Switch on the instrument and check that the batteries are satisfactory.

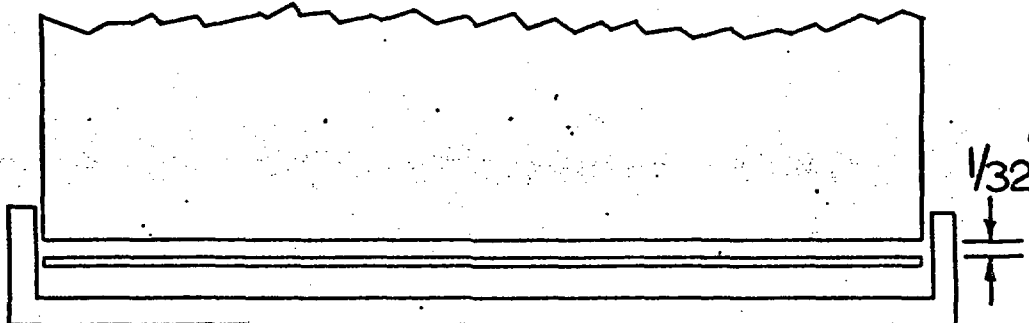


FIG. 6-1 CALIBRATION JIG

7. Switch to the 100K range.
8. Note the reading on the meter scale. It should be 60,000 cpm.
9. Note the reading on the electrostatic voltmeter. It should be between 950 and 1,250 volts.
10. Note the reading on the VTVM. It should be greater than 100 millivolts.
11. If the reading at step 8 is not 60,000 cpm then adjust R14 until it is. If, in order to get a reading of 60,000 cpm, the reading of step 10 is reduced to less than 100 millivolts then FULL CALIBRATION must be performed except that a lower voltage tap should not be used.

**NOTE**

The instrument normally will be calibrated against plutonium 239 sources such that a source with a distribution equivalent to 1000  $\mu\text{g}/\text{m}^2$  will produce an indication of 100,000 cpm. Consequently, the desired indication is the plutonium source activity in micrograms per square meter times one hundred. Except for this note all calibration procedures herein are based on this instrument response unless a 2 pi calibration is specifically requested by the user. For a 2 pi calibration, the desired indication is the plutonium source activity in micrograms per square meter times 116. All procedures and adjustments, except for the desired meter reading, apply to either a "normal" or a 2 pi calibration. Equipment maintenance sheets should indicate whenever a 2 pi calibration is made.

"Normal Calibration"    "2 pi" Calibration

I = 100A

I = 116 A

Where I = Desired meter indication in cpm.

A = Plutonium source activity in  $\mu\text{g}/\text{m}^2$

**d. Full Calibration**

1. Perform steps 1 through 5 of the partial calibration.
2. Connect the lead from pin 6 of the printed board connector J4 to the lowest voltage position of the transformer tertiary winding (terminal 6). Initially this lead may be connected to terminal 6, 7, or 8.

3. With this tap wired in the circuit perform steps 6 through 10 of the PARTIAL CALIBRATION.

4. If the instrument cannot be calibrated then successively higher transformer taps (terminal 7 and 8 respectively) should be selected.

5. If, when the highest tap has been selected (terminal 8), the instrument still cannot be calibrated then resistor R-33 should be short circuited and steps 1 through 4 of the FULL CALIBRATION repeated.

e. Range Check - To check the correspondence between ranges and to determine the accuracy of the other ranges the RANGE CHECK should be performed.

1. Replace the 600  $\mu\text{g}/\text{m}^2$  source by the 6  $\mu\text{g}/\text{m}^2$  source and switch to the 1K range. The instrument reading should be 600 cpm  $\pm$  20%.

2. Switch to the 10K range and replace the 6  $\mu\text{g}/\text{m}^2$  source by the 60  $\mu\text{g}/\text{m}^2$  source. The instrument reading should be 6000 cpm  $\pm$  20%.

3. Switch to the 1M range and replace the 60  $\mu\text{g}/\text{m}^2$  source with the 6000  $\mu\text{g}/\text{m}^2$  source. The instrument reading should be 600,000 cpm  $\pm$  20%.

f. Noise Check

1. Remove all alpha sources from close proximity to the sensitive element.

2. Plug in the headset.

3. Switch the instrument on.

4. The noise background should be less than 15 cpm as measured by the headset.

**NOTE**

A noise reading up to 150 cpm will occasionally be measurable on the meter on the 0-1000 cpm range.

**6-4. REPAIR AND REPLACEMENT OF PARTS**

a. General - Radiac Set AN/PDR-56A has been designed with ease of repair in mind. No special tools are required. A "pencil" type soldering iron will be useful. A heat sink

Supplement 4A

The attached sheets are copies of pages of the technical manual for the AN/FDR-56.

## SECTION 3 OPERATOR'S SECTION

### CAUTION

The Thorium Check Source, which is located on the underside of the radiacmeter case, should always be handled with extreme care. This source is of metallic form and is not subject to wiping off or flaking, however, IT SHOULD NEVER BE TOUCHED WITH A SHARP OBJECT WHICH COULD SCRATCH OR ABRASE IT.

### 3-1. FUNCTIONAL OPERATION

Radiac Set AN/PDR-56A is used to measure alpha radiation up to an intensity of  $10^6$  counts per minute. The Radiac Set consists of two principal parts, the Radiacmeter IM-160A/PDR-56 and the Probe DT224/PDR-56. The primary source of power is two 1-1/2 volt batteries. A regulated power supply produces -4 and -10V for the transistor circuits and -1000 volts (nominal) for the Photomultiplier Tube. In addition, the radiacmeter consists of a Schmitt trigger, a buffer inverter and a count rate circuit. The output of this last circuit is measured on the meter or indicated by clicks in the headphones. The probe uses a silver activated zinc sulphide screen as a scintillator. An alpha particle, with energy greater than the detection threshold (about 3 MeV), which is incident to this screen produces a pulse of light. This light pulse is conducted to the photocathode of a photomultiplier tube by a lucite light pipe. This results in the emission of photo-electrons which, due to secondary emission, produce a sufficiently large pulse at the plate of the photomultiplier tube to trigger the Schmitt discriminator via an emitter follower.

The meter output is proportional to the intensity of the alpha contamination.

To check the operation of the instrument a metallic Thorium check source is supplied. This is located beneath the radiacmeter case, see figure 3-2. When the probe is correctly positioned the meter reading is about  $32,000 \pm 8000$  cpm ( $0-10^5$  c.p.m. range). The source is not

intended as a primary calibration standard, but a reasonable estimate of instrument accuracy can be obtained provided the source is clean and dry and the same detector-source geometry is used each time the equipment is checked.

### 3-2. ALPHA RADIATION

The monitoring of the alpha radiation entails the detection of a highly ionizing particle with a short range.

Alpha particles are easily absorbed losing energy by excitation and ionization of the absorber atoms. Generally this can be accomplished by a sheet of paper, by an aluminum foil 0.0015 inches thick or by a few inches of air.

If the particles emitted by an alpha source, in air, are counted by a scintillation method it is found that their number decreases gradually up to a certain distance from the source, after which the reading falls off sharply. This distance is called the range and is related to the initial energy of the particle.

The most energetic natural alpha particle, 10.5 MeV, has a range of only 4 inches in air. An alpha particle of greater than 7.5 MeV is necessary to penetrate the outer layer of dead skin. Since only a few short lived isotopes emit alpha radiation of these energies, the biological hazard from particles is strictly internal.

For alpha radiation having energies between 4 and 7 MeV the particle range in air can be calculated from the formula.

$$R = 0.12E^{3/2}$$

Where R is the mean range of the particle in inches and E is the energy of the particle in MeV.

Typical ranges in air of the more important isotopes associated with nuclear energy are given in the following table:

d. CALIBRATION ADJUSTMENTS. There are no calibration adjustments for the operator.

c. PRECAUTIONS.

Batteries - When installing the batteries observe the polarity indication on the case of the battery and the battery well. The condition of the batteries in the equipment should be checked at least once every thirty days. Batteries which are not satisfactory (step 5, paragraph 3-3) should be removed immediately and replaced with fresh batteries.

Radiation Hazard - Extreme caution must be exercised when handling alpha materials. These materials can be extremely hazardous when introduced into the biological system. This can be done by ingestion, inhalation or by absorption through a break in the skin. Alpha activities generally consist of very heavy nuclei which have a strong tendency to concentrate in the bone and can cause severe local tissue destruction. Most alpha emitting isotopes have extremely long biological half lives and thus have a tendency to remain fixed in the body.

### 3-5. OPERATOR'S MAINTENANCE

a. OPERATION CHECK

Step 1 - Turn the selector switch to BATT. The meter reading should be greater than the vertical mark at the extreme left of the BATT section. If the meter reading is less than this replace the batteries.

Step 2 - Switch the selector switch to the 1K position and plug in the earphones. In the absence of alpha radiation two things will be heard. There will be a high pitched whine from the pulse transformer and an occasional click indicating background. The background may cause a meter reading of less than 50 c.p.m.

Step 3 - Switch to the 100K position. Invert the probe and place the slotted underface against the Thorium check source using the gap in the positioning runners (Reference Figure 3-1).

The meter reading should be  $32,000 \pm 8000$  cpm. The clicks in the headphone should be loud and fast. If the main probe is now slowly separated from the check source the meter reading will decrease and the clicks become less frequent. At a separation distance of two to three inches no indication from the Thorium check source will be observed.

If the phenomena associated with step 3 are evident the instrument is functioning satisfactorily.

#### NOTE

If excessive readings are indicated without the presence of alpha radiation it is probable that the light integrity of the window has been impaired. This can be checked by turning the probe base towards a light and observing the increase in reading. Under no circumstances should a strong light be placed close to the probe base as, if the screen has been punctured, the photomultiplier tube will be saturated and damaged. For emergency repairs the screen may be patched with an opaque material such as black tape. This will result in a reduction of efficiency and hence a reduction of count rate.

b. EMERGENCY MAINTENANCE. In the event that the instrument does not function correctly it should be returned for base maintenance. If the probe is opened to the light the screen and phototube will phosphoresce causing unusually high background and calibration drift for up to two hours rendering the instrument unreliable during this period.

## SECTION 5 TROUBLE SHOOTING

### CAUTION

The Thorium Check Source, which is located on the underside of the radiac-meter case, should always be handled with extreme care. This source is of metallic form and is not subject to wiping off or flaking, however, IT SHOULD NEVER BE TOUCHED WITH A SHARP OBJECT WHICH COULD SCRATCH OR ABRASE IT.

### 5-1. GENERAL

Trouble shooting of the radiac set will be easier if an orderly procedure is used. This section describes the symptoms produced by malfunctioning of the radiac set and the procedures used for localizing troubles by aural and visual means.

Note that the operation of the radiacmeter probes and headset can be checked with the radio-active test source on the bottom of the radiac-meter case. This test will yield a qualitative estimate of the performance of the equipment; however, the absolute accuracy of the calibration cannot be determined by this means.

### 5-2. TEST EQUIPMENT REQUIRED

The following equipment will be required for servicing the Radiac Set AN/PDR-56A.

- a. Oscilloscope AN/USM-24
- b. AN/USM-116A, Electronic Voltmeter
- c. Alpha Sources (see para. 6-3)
- d. Electrostatic voltmeter 0-1500 volts

### 5-3. OVERALL TROUBLE SHOOTING

(Refer to Figs. 3-2, 5-2, 5-3 and 6-2)

a. Preliminary Check - Before proceeding with any electrical tests the following mechanical inspection procedure should be followed:

1. The instrument case should be examined for any mechanical damage.
2. The selector switch should be turned to its various positions to see that it indexes properly.
3. The meter should be examined. Observe the meter needle to see that it is not bent. Check the mechanical zero of the meter. The zero may be set when the radiacmeter is opened.

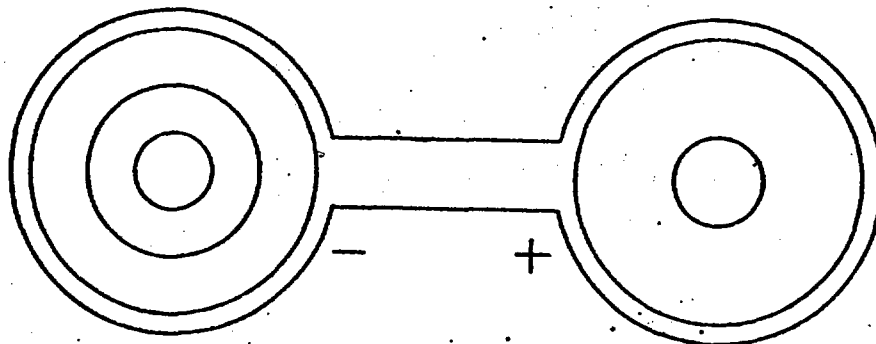


FIG. 5-2 BATTERY POLARITY

## SECTION 5 TROUBLE SHOOTING

### CAUTION

The Thorium Check Source, which is located on the underside of the radiac-meter case, should always be handled with extreme care. This source is of metallic form and is not subject to wiping off or flaking, however, IT SHOULD NEVER BE TOUCHED WITH A SHARP OBJECT WHICH COULD SCRATCH OR ABRASE IT.

### 5-1. GENERAL

Trouble shooting of the radiac set will be easier if an orderly procedure is used. This section describes the symptoms produced by malfunctioning of the radiac set and the procedures used for localizing troubles by aural and visual means.

Note that the operation of the radiacmeter probes and headset can be checked with the radio-active test source on the bottom of the radiac-meter case. This test will yield a qualitative estimate of the performance of the equipment; however, the absolute accuracy of the calibration cannot be determined by this means.

### 5-2. TEST EQUIPMENT REQUIRED

The following equipment will be required for servicing the Radiac Set AN/PDR-56A.

- a. Oscilloscope AN/USM-24
- b. AN/USM-116A, Electronic Voltmeter
- c. Alpha Sources (see para. 6-3)
- d. Electrostatic voltmeter 0-1500 volts

### 5-3. OVERALL TROUBLE SHOOTING

(Refer to Figs. 3-2, 5-2, 5-3 and 6-2)

a. Preliminary Check - Before proceeding with any electrical tests the following mechanical inspection procedure should be followed:

1. The instrument case should be examined for any mechanical damage.
2. The selector switch should be turned to its various positions to see that it indexes properly.
3. The meter should be examined. Observe the meter needle to see that it is not bent. Check the mechanical zero of the meter. The zero may be set when the radiacmeter is opened.

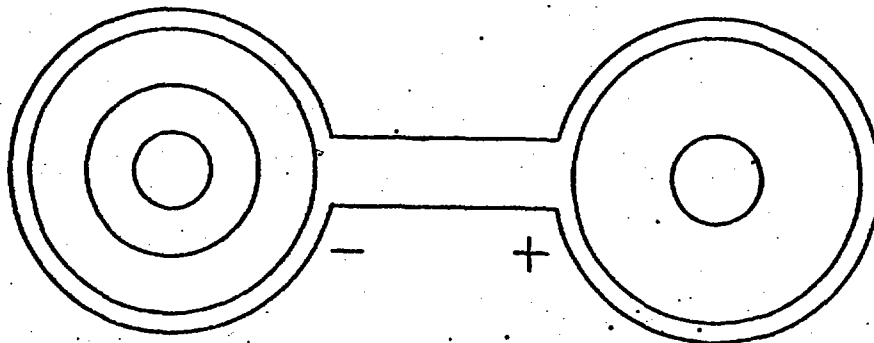


FIG. 5-2 BATTERY POLARITY

## SECTION 6 SERVICE AND REPAIR

### CAUTION

The Thorium Check Source, which is located on the underside of the radiacmeter case, should always be handled with extreme care. This source is of metallic form and is not subject to wiping off or flaking, however, IT SHOULD NEVER BE TOUCHED WITH A SHARP OBJECT WHICH COULD SCRATCH OR ABRADÉ IT.

### 6-1. FAILURE REPORT

Report each failure of the equipment, whether caused by a defective part, wear, improper operation, or an external cause. Use your **ELECTRONIC FAILURE REPORT** form. Each pad of the forms includes full instructions for filling out the forms and forwarding them to the Bureau of Ships. However, the importance of providing complete information cannot be emphasized too much. Be sure that you include the model designation and serial number of the equipment (from the equipment identification plate), the type number and serial number of the major unit (from the major unit identification plate), and the type number and reference designation of the particular defective part (from the technical manual). Describe the cause of the failure completely, continuing on the back of the form if necessary. Do not sacrifice clarity for brevity. And remember - there are two sides to the failure report. ---

### "YOUR SIDE"

Every **FAILURE REPORT** is a boost for you:

1. It shows that you are doing your job.
2. It helps make your job easier.

3. It insures available replacements.
4. It gives you a chance to pass your knowledge to men on the team.

### "BUREAU SIDE"

The Bureau of Ships uses the information to:

1. Evaluate present equipment.
2. Improve future equipment.
3. Order replacements for stock.
4. Prepare field changes.
5. Publish Maintenance Data.

Always keep a supply of failure report forms on board. You can get them from the nearest District Publications and Printing Office.

### 6-2. PREVENTATIVE MAINTENANCE

a. **General - Preventive maintenance** is maintenance performed on equipment (usually when the equipment is not in use) to keep it in good working order so that there will be minimum interruptions in service. Preventive maintenance differs from trouble shooting and repair in that its object is to prevent the occurrence of troubles.

b. **Routine Maintenance Check Chart** - The procedures listed in Table 6-1 are to be performed at the intervals indicated, unless these intervals are modified by the officer in charge.

TABLE 6-1 ROUTINE MAINTENANCE CHECK CHART

What to Check	When to Check	How to Check	Precautions
Battery Condition	Monthly	Turn function switch to BATT. Meter reading should be greater than the minimum as indicated by vertical mark at the extreme left of the BATT. section.	Return range switch to OFF after test.
Exterior front panel Radiac set	Monthly	Wipe with clean dry cloth, removing all dirt and dust.	Do not touch <u>Thorium check source</u> .
Radiacmeter front panel screws	Monthly	Screws should seat firmly.	Do not tighten excessively. A loose screw will permit leakage of the case.
Probe Screws	Monthly	Screws should seat firmly.	Do not tighten excessively. A loose screw will permit leakage of the case.
Range Switch Knob	Monthly	If knob is loose tighten with Allen wrench.	Do not tighten excessively.
Handle, captive Screw	Monthly	Adjust to finger tightness	None
Radiacmeter Circuit	Monthly	See para. 3-4	Do not touch <u>Thorium check source</u> .
Headset	Monthly	Remove dirt, check tightness of screws and connections.	None

### 6-3. PERFORMANCE STANDARDS

#### WARNING

**CALIBRATION OF THE RADIAC SET, AN/PDR-56A MAY BE UNDERTAKEN ONLY BY QUALIFIED RADIAC REPAIR PERSONNEL AT AN AUTHORIZED FACILITY.**

a. General - Radiac Set AN/PDR-56A was calibrated when manufactured and complete calibration is not usually required unless certain critical components are replaced. Calibration should not be attempted until the Radiac Set has been stabilized at room temperatures. In addition,

it should be allowed to run for approximately 20 minutes before any adjustment. If the PM tube has been changed or the probe opened, no adjustment should be made for at least 2 hours and preferably the probe should be dark acclimated overnight.

b. Calibration - Recalibration must always be performed when the following critical components are changed

1. Printed Circuit boards (A1, A2, A4)
2. PM Tube (V1)
3. Light pipe and screen (MP5)
4. Transformer (T1)

(eg. long-nose pliers or alligator clips) are required when soldering semiconductors. Care should be taken when soldering to apply a minimum of heat and to avoid burning nearby leads and components. Disturb lead dress as little as possible. Take care during servicing to

- a. Not rupture the aluminized mylar screen
- b. Keep foreign matter out of the instrument
- c. Not introduce phosphorescent materials into the probe. This includes a grease or oil film on the PM tube or light pipe, glues and resins for bonding.

d. Not scratch the Thorium check source.

b. Removal of the PM Tube

1. Detach the radiacmeter from the probe by unscrewing the handle captive screw.
2. Loosen the two screws that keep the probe cover and emitter follower assembly together.
3. Separate the probe cover and emitter follower assembly. It may be necessary to turn radially to overcome the resistance of the "O" ring humidity seal on the emitter follower assembly.
4. Hold the tube by its plastic base and pull it out of its socket.

c. Removal of the Light Pipe and Aluminized Mylar Screen

1. Detach the radiacmeter from the probe by unscrewing the handle captive screw.
2. Loosen the six captive screws that hold the probe cover and the probe base plate together and separate them.
3. With an open ended wrench loosen the two forward end clamps.
4. With a screwdriver loosen the two rear end clamps and the two side clamps.
5. Loosen the two long screws that hold the light pipe onto the probe base plate.
6. The light pipe can now be removed.
7. When the light pipe has been removed

the aluminized mylar screen can be taken out.

8. When replacing ensure that the rubber gasket and aluminized mylar screen are seated properly and that the light pipe is properly aligned with the slots in the probe base plate.

d. Dismantling the Components Mounted on the Panel

1. Detach the radiacmeter from the probe by unscrewing the handle captive screw.
2. Loosen the six captive screws that hold the panel to the box and separate them.
3. With a 1/4" open end wrench, remove the nuts from the rods which hold the printed boards A1 and A2. Remove the rods and spacers. Plug-in assembly A1 or A2 can now be grasped by the edges and worked out of the socket.
4. Next the Printed Circuit Boards Mounting Frame should be removed. This is done by loosening the two screws that hold it to the battery well bosses and the three screws that hold it to the support bracket.
5. The two printed circuit assemblies A3 and A4 are held together by the trimpot mounting bracket and the spacer.
6. The plug-in assembly A3 is secured to the Printed Circuit Board Mounting Frame by a block near the plug-in connector and by two spacers. If the screws holding these spacers are loosened the assembly may be withdrawn from the connector.
7. To remove the meter scale chain, detach the spring from the chain. The sprockets may be removed by loosening the two Allen socket screws on each sprocket.
8. The only components still mounted to the panel are the transformer, the switch and the meter.
9. The transformer is mounted to the panel by two screws.
10. To remove the switch, first, take off the knob by loosening the two Allen socket screws. Remove the nut that screws onto the switch bushing. The switch can now be freed from the panel.
11. The meter is mounted to the panel by four screws. Two forward screws mount the meter light assembly.

TABLE 7-1 PARTS LIST (Cont'd.)

Ref. Desig.	Name and Description	Locating Function
MP14	Plate, Identification. Aluminum foil, pressure sensitive, silver letters on orange background inscribed "AN/PDR-56A, RADIAC SET" Tracerlab Part No. B238019	Radiac Set Nameplate, side of carrying case
MP15	Plate, Identification. Aluminum foil, pressure sensitive, silver letters on black background inscribed "CY-2839/PDR-56, CASE, RADIAC SET" Tracerlab Part No. B238020	Carrying case nameplate, side of carrying case
MP16	Calibration Source - Alpha Source - Thorium 232 sheet 2-1/4" x 2-3/4" x 2-3/4" x .020" thick, 25 gms/unit Tracerlab Part No. B238027	Bonded to underneath of main case
MP17	PM Tube Housing, Aluminum, grey enamel Tracerlab Part No. C237980	Between handle and main probe
MP18	Same as MP1	Seal to S3
MP19	Sprocket wheel, stainless steel, 16 teeth, pitch .1475 ins., two holes tapped 4-40 Tracerlab Part No. B239997	Switch/Meter Drive
MP20	Chain, micropitch, non-magnetic st. st. bushing link at both ends. 47 pitches, .1475 pitch, Tracerlab Part No. B238015	Same as MP19
MP21	Spring, extension, 3/4 ins. long: 3/16 ins. OD .031 diam. music wire. Tracerlab Part No. B240000	Same as MP19
MP22	Receptacle Cover, brass, silver plated, mounts for bayonet locking MIL-C-3608 Type CW-123A/U, Amphenol	Covers phone connector
MP23	PM tube housing assembly - emitter follower assembly potted in PM tube housing (MP17), Tracerlab Part No. C238021	Between handle and Main Probe
MP24	Deleted	
MP25	Cover Gasket, Tracerlab Part No. B238688	Auxiliary Probe
MP26	Deleted	
MP27	Deleted	

## Supplement Five

ADD:

Source C. Although directives specify no requirements of training or experience for personnel using the radiac instruments AN/PDR-56, of which these sources are a part, individuals using these instruments are ordinarily, as a minimum, members of a unit chemical-biological-radiological (CBR) team. Membership in a unit CBR team carries a requirement for 10 hours of CBR training, which includes use of the radiac instrument, and at least a brief amount of training in radiation safety and radioactivity measurement. Use of these instruments is supervised by the unit CBR officer or CBR non-commissioned officer, who have at least 12 hours of training in radiation safety and radioactivity measurement. In the event of an accident involving the source material the local radiological protection officer (RPO), is notified. He is responsible for the radiation protection program of the user activity or unit. The local RPO has radiation safety training equivalent to the 3 weeks Radiological Safety course given at Fort McClellan, Alabama.

Supplement Six

ADD:

Source C. Local radiation survey programs and procedures are prescribed by local radiation protection officers (RPO's) who are responsible to their commanding officers to prevent radiological contamination and insure that requirements listed in the technical manual for the AN/PDR-56 are fulfilled. Overall quality surveillance is maintained by 3 or more items being evaluated annually for functional and radiological safety considerations at either Lexington Blue Grass Army Depot, Lexington, Kentucky, or at US Army Electronics Command, Fort Monmouth, New Jersey.